Stochastic many-particle model for LFP electrodes

Continuum Mechanics and Thermodynamics manuscript No.
(will be inserted by the editor)

Stochastic many-particle model for LFP-electrodes

Clemens Guhlke · Paul Gajewski · Mario Maurelli · Peter K. Friz · Wolfgang Dreyer

Received: date / Accepted: date

Abstract In the framework of non-equilibrium thermodynamics we derive a new model for many-particle electrodes. The model is applied to $LiFePO_4$ (LFP) electrodes consisting of many LFP particles of nanometer size. The phase transition from a lithium-poor to a lithium-rich phase within LFP electrodes is controlled by both different particle sizes and surface fluctuations leading to a system of stochastic differential equations.

An explicit relation between battery voltage and current controlled by the thermodynamic state variables is derived. This voltage-current relation reveals that in thin LFP electrodes lithium intercalation from the particle surfaces into the LFP particles is the principal rate limiting process. There are only two constant kinetic parameters in the model describing the intercalation rate and the fluctuation strength, respectively. The model correctly predicts several features of LFP electrodes, viz. the phase transition, the observed voltage plateaus, hysteresis and the rate limiting capacity. Moreover we study the impact of both the particle size distribution and the active surface area on the voltage-charge characteristics of the electrode. Finally we carefully discuss the phase transition for varying charging/discharging rates.

Keywords lithium-ion battery · lithium iron phosphate · phase transitions · many particle electrode

1 Introduction

In recent years there is an increasing need for powerful and effective batteries due to rapidly growing electro mobility. Currently the most promising battery

Weierstrass Institute
Mohrenstr. 39
10117 Berlin
Germany
E-Mail: clemens.guhlke@wias-berlin.de

type are lithium-ion batteries. In the last decades great progress has been made in the development of both new electrode materials and new electrolytes. In order to design and improve the batteries a deep understanding of their physicochemical processes is mandatory. To this end mathematical models embodying the physical and chemical behavior of battery materials from the micro to the macro scale are essential.

Many classical continuum models for lithium-ion batteries rely on the framework developed by Newman et al. [10,11,43]. Here the processes within electrodes and electrolytes are described by diffusion equations and the transfer of charge at the electrode-electrolyte interface is modeled by Butler-Volmer kinetics [25,28,41,21,23]. For known model parameter, these models are capable to determine the influence of the battery geometry on the cell voltage and thus to configure a suitable battery design. Although the Newman battery models are quite popular and widely used they exhibit several drawbacks, which limits the usability of these models:

- The model parameters are functions of concentration and temperature. Thus a costly parameter fitting is necessary to have accordance with measurements.
- The dependence of the open-circuit potential of the battery on the state of charge is a fitting curve and is not predicted by the battery model itself.
- The Newman model is based on the electroneutral approximation in the electrolyte phase, which is not valid in porous electrodes with pore diameters in the range of the Debye length.
- For phase separating electrode materials the incorporation of phase transition within the Newman model is challenging.
- The momentum balance is ignored. Thus the extension of Newman models to volume expansion and elasticity is severely limited.
- The validity range of the Newman model is not defined. In the case of failure of the model, the origin of the failure can not be identified and an improvement/extension of the model is difficult.

These drawbacks might be resolved if the battery model is embedded in a general theoretical framework like non-equilibrium thermodynamics. The use of non-equilibrium thermodynamics has the advantage that it distinguishes carefully between universal principles and material dependent constitutive relations. Thus this offers the chance to formulate quite general constitutive equations where the material properties are encoded within a general free energy function. Moreover, numerous different phenomena can be consistently coupled [36,7,39,3]. In recent years continuum models for batteries and electrodes could be improved significantly by applying non-equilibrium thermodynamics [2,33,42,31,32,14,20,15].

In this study we develop a general mathematical model for many-particle electrodes in the context of non-equilibrium thermodynamics, which takes into account diffusion and elastic deformations in the electrode particles and the electrolyte as well. Particularly, adsorption, reactions and surface tension at the electrode-electrolyte interface are incorporated. For nano-sized electrode

particles and electrode widths in the micrometer scale, the general electrode model can be simplified in such a way that the processes within the many-particle electrode are dominated exclusively by surface phenomena: adsorption, intercalation and reaction. Finally we apply the model to a lithium iron phosphate (LFP) electrode.

The modeling of LFP represents a challenge because during charging and discharging LFP exhibits a two-phase system with lithium-rich and lithium-poor phases [40,8,5]. The characteristic horizontal voltage plateaus in the voltage-capacity diagram is due to this phase transition, Figure 1_{right}. Here the task to design a model becomes ambitious since two different phase transitions are in competition [20]: (i) There is a phase transition in the individual particles, and (ii) a phase transition in the ensemble of storage particles, where the LFP particles have high and low lithium filling, respectively. Moreover, the phase transition happens in a sequential order, in other words, the particles are filled according to the rule *one after the other* [20]. Detailed studies of the phenomenon have revealed that the kind of phase transition depends on the charging speed and the size of the storage particles [33,35,34,5]. Careful experimental studies unambiguously show that the time scale of the phase transition within a nano-sized particle is much smaller than the charging time of a battery [34]. Thus on the time scale of charging the phase transition within the ensemble of nano-sized particles is the dominant one.

In this study we only address the phase transition within the ensemble. We incorporate in our many-particle model two stochastic mechanisms which might affect the phase transitions: i) distribution of particle volumes and effective surface areas over the particle ensemble and ii) stochastic fluctuations on the surface. At the end the LFP many particle model is represented by a system of stochastic differential equations. Despite its simplicity the many-particle model embodies already many properties of LFP electrodes. In particular we may predict the influence of size distribution (of the electrode particles), active surface area, surface stochastic fluctuations and charging rate on the battery voltage.

The paper is organized as follows. We start in Section 2 with a phenomenological description of the functionality of a battery consisting of a LFP electrode as cathode and a metallic lithium electrode as anode. The stochastic model is introduced in Section 3. In Section 5 we discuss the relation between the phase transition and the battery voltage on the basis of a variety of simulations. The detailed derivation of the model equations including a list of the essential assumptions is described in Section 6. The paper concludes with a discussion, where in particular we address the initially mentioned drawbacks of current battery models. A list of model parameters and symbols is given at the end.

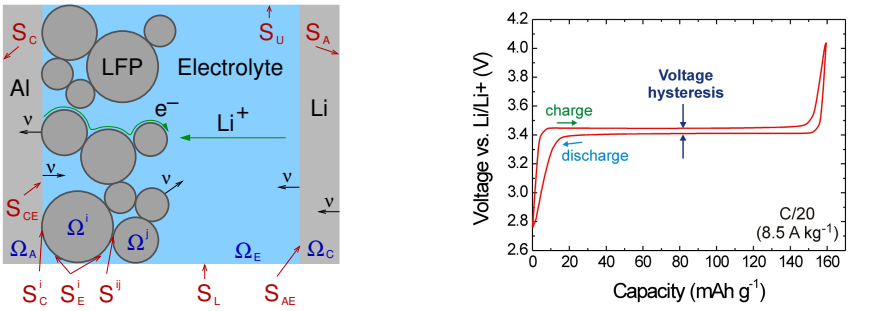

Fig. 1 Left: Sketch of the LFP battery, Right: Typical voltage-capacity profile for a LFP electrode at low charging/discharging rate C/20 (from [20])

2 Description of the battery

Design of the battery. We consider a battery consisting of a LFP many-particle cathode, a liquid electrolyte and metallic lithium as the anode. The many-particle electrode consists of carbon coated LFP particles. The carbon coating improves the electric conductivity of the LFP particles [38,9]. Usually carbon black is added to the LFP electrode such that the particles are electrically connected to each other. We neglect the carbon black and model the electron transport by the assumption that carbon coated LFP particles form an electric network. Thus the electron transport is achieved along the carbon coated particle surfaces. Moreover some LFP-particles are attached to a metal based current collector. Here usually aluminum is utilized. The electrolyte is a mixture of some lithium salt dissolved in some liquid organic solvent, e.g. $LiPF_6$ dissolved in a mixture of ethylene and dimethyl carbonate. The passive components of the battery such as binder, separator and further additives are ignored in this study. A sketch of the battery is shown in Figure 1.

Processes within the battery. During discharging of the battery lithium is transferred from the lithium anode to the LFP many particle cathode and vice versa for thecharging process. The transport of lithium is the main limiting phenomenon that controls the functionality of the battery. The transport process itself consists of a combination of several rate limiting phenomena. In particular, we have to distinguish between surface and bulk transport. The main bulk phenomena are ion diffusion within the liquid electrolyte and lithium diffusion and phase separation within the LFP particles.

At the particle surface we have: i) tangential mass transport, in particular electron transport, ii) adsorption of electrolytic species, iii) an electron transfer reaction of the form $Li^+ + e^- \rightleftharpoons Li$, and iv) the intercalation of lithium into the iron-phosphate lattice.

At the lithium anode the situation is more simple. Lithium is deposited on or dissolved from the electrode surface for the charging and the discharging process, respectively.

Further processes such as heat generation and transport, mechanical deformation, dendrite growth or aging processes are not among the topics of this work.However, the thermodynamic approach of Sect. 6 can be used to incorporate these phenomena as well.

Model restrictions. Our many-particle model for a LFP electrode describes the experimentally observed features of the battery and is easy to solve. We restrict and simplify the full thermodynamic model of Sect. 6 by some assumptions. The main assumptions are:

- Large porosity of the LFP electrode, whose thickness is in the micrometer scale.
- Nano-sized LFP particles.
- Rigid LFP particles, i.e. volume and surface of a particle do not change for a varying charging state.
- Constant temperature due to high heat conduction, which is appropriate in small cells.
- Lithium is exclusively stored in the LFP particles and in the lithium anode.
- The lithium anode is equipped with a large surface.
- Fast surface diffusion.

The full and more detailed list of assumptions can be found in Sect. 6. The main implications of these assumptions are that the lithium mole fraction within a particle is spatially constant and the electrolyte behaves quasi-static, i.e. the lithium and charge transport within the particles and the electrolyte is infinitely fast on the time scale of charging.

These assumptions about the battery are satisfied for micro batteries and high power batteries as well. However, for moderate charging-discharging times there is a much larger class of batteries where the assumption are appropriate.

3 The many-particle model

In this section we introduce the many-particle model for the LFP electrode. The model consists of (i) a system of stochastic differential equations (SDE), (ii) a constraint prescribing the state of charge of the battery, and (iii) voltage and current relations.

We split the introduction of the many-particle model into two parts. In the first part we introduce the "semi-stochastic" model, where stochastic effects enter via distributions of volumes and surface areas into the model. In the second part we specify the full stochastic model, where stochastic fluctuations modeled by Wiener processes are added. The detailed derivation of the model is postponed to Sect. 6.

Notations. The many-particle electrode consists of N_{P} storage particles indexed by $i = 1, 2, ..., N_{\mathrm{P}}$. The particles have volumes V^i and active surface

areas $A_{\mathtt{E}}^i$, which are time independent due to the model assumption. The total volume and the total active surface area of the LFP particles are denoted by

$$V_{\mathtt{P}} = \sum_{i=1}^{N_{\mathtt{P}}} V^i \qquad \text{and} \qquad A_{\mathtt{E}} = \sum_{i=1}^{N_{\mathtt{P}}} A_{\mathtt{E}}^i \ . \tag{1}$$

The surface area of the lithium anode/electrolyte interface is denoted by $A_{\mathtt{AE}}$.

Thermodynamic state. The number of stored lithium atoms in particle P_i at time $t \geq 0$ is denoted by $\mathcal{N}_{\mathrm{Li}}^i(t)$. The number of $FePO_4$ units forming the matrix lattice of particle P_i is time independent and denoted by $\mathcal{N}_{\mathrm{FePO_4}}^i$. Each particle has the same time independent number density $n_{\mathrm{FePO_4}}$. The number densities of the intercalated lithium n_{Li}^i are time dependent but constant in space within a particle P_i. The number densities are related to the number of stored lithium and to the number of $FePO_4$ units by $\mathcal{N}^i(t) = n_{\mathrm{Li}}^i(t)V^i$ and $\mathcal{N}_{\mathrm{FePO_4}}^i = n_{\mathrm{FePO_4}} V^i$.

Each $FePO_4$ unit provides a free lattice site that may be occupied by a lithium atom. Then the *mole fraction* $y^i \in [0,1]$ of occupied lattice sites of particle P_i is defined as

$$y^i(t) = \frac{n_{\mathrm{Li}}^i(t)}{n_{\mathrm{FePO_4}}} \ . \tag{2}$$

The thermodynamic state of the many-particle electrode is exclusively represented by the lithium mole fractions of the particles, $(y^i)_{i=1,2,\dots,N_{\mathtt{P}}}$.

3.1 The semi-stochastic model for many particle electrodes

The evolution of the thermodynamic state of the many-particle electrode is described by the system

$$\frac{dy^i}{dt} = \frac{1}{\tau^i}\frac{m_{\mathrm{Li}}}{k_B T}(\mu_{s,\mathrm{Li}} - \mu_{\mathrm{Li}}(y^i)) \qquad \text{with} \quad \frac{1}{\tau^i} = \frac{k_{\mathrm{Li}}}{m_{\mathrm{Li}} n_{\mathrm{FePO_4}}}\frac{A_{\mathtt{E}}^i}{V^i} \ . \tag{3}$$

As shown in Sect. 6 the system (3) relies on the integrated mass balance equations of the stored lithium in the LFP particles. Due to the assumption of homogeneous lithium mole fractions, the particle volume V^i and the active surface area $A_{\mathtt{E}}^i$ appear explicitly in the equation. This leads to particle size dependent relaxation time τ^i for each particle.

The right hand site of (3) arises from the flux j_{Li}^i describing the intercalation of lithium atoms from the surface of particle P_i into the $FePO_4$ lattice,

$$j_{\mathrm{Li}}^i = k_{\mathrm{Li}} \tfrac{m_{\mathrm{Li}}}{k_B T}\big(\mu_{\mathrm{Li}}(y^i) - \mu_{s,\mathrm{Li}}\big) \ . \tag{4}$$

The lithium flux is driven by the chemical potential difference $\mu_{\mathrm{Li}}(y^i) - \mu_{s,\mathrm{Li}}$, where $\mu_{s,\mathrm{Li}}$ represents the surface chemical potential of lithium atoms on the particle surface and μ_{Li} is the chemical potential of intercalated lithium at the surface. The kinetic parameter k_{Li} has the unit $\mathrm{kg/(m^2 s)}$ and represents the

rate constant of intercalation of lithium atoms into the $FePO_4$ lattice. m_{Li} is the molecular mass of lithium and $n_{\mathrm{FePO_4}}$ is number density of iron phosphate.

The assumption of fast surface diffusion implies that the surface chemical potential $\mu_{s,\mathrm{Li}}$ is the same for all LFP particles. Therefore all balance equations are coupled through the chemical potential $\mu_{s,\mathrm{Li}}$. The chemical potential of intercalated lithium, μ_{Li}, is a function of the lithium mole fraction y^i of the corresponding LFP particle. In order to model the phase separating behavior of Li_yFePO_4 we choose the widely used non-monotone function [42, 1, 14]

$$\mu_{\mathrm{Li}} = \mu_{\mathrm{Li}}^{\mathrm{ref}} + \tfrac{L}{m_{\mathrm{Li}}}(1-2y) + \tfrac{k_B T}{m_{\mathrm{Li}}} \ln\left(\frac{y}{1-y}\right) . \tag{5}$$

The chemical potential consists of three contributions. The first part $\mu_{\mathrm{Li}}^{\mathrm{ref}}$ is a constant material parameter depending on the properties of $LiFePO_4$. The second part takes into account the energetic interaction of lithium with the iron-phosphate lattice. The parameter L represents the heat of solution and has the unit J (Joule). In particular, the parameter L controls the energy barrier between the lithium-poor and the lithium-rich phase[14]. Finally there is a third contribution that takes into account the entropy of mixing of lithium atoms on the available lattice sites. Figure 2 depicts the chemical potential function $\mu_{\mathrm{Li}}(y)$ for a typical choice of $L = 94.4 \times 10^{-22}$J/kg and $\mu_{\mathrm{Li}}^{\mathrm{ref}} = 0$ J/kg .

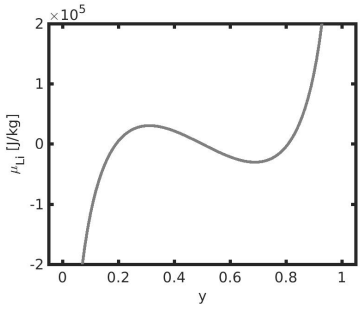

Fig. 2 Non-monotone chemical potential of lithium in iron-phosphate.

State of charge - charging rate. The *total mole fraction* $q \in [0,1]$ of the many-particle ensemble describes the *state of charge* of the battery,

$$q(t) = \frac{\sum_{i=1}^{N_{\mathrm{P}}} \mathcal{N}_{\mathrm{Li}}^i(t)}{\sum_{j=1}^{N_{\mathrm{P}}} \mathcal{N}_{\mathrm{FePO_4}}^j} = \sum_{i=1}^{N_{\mathrm{P}}} \frac{V^i}{V_{\mathrm{P}}} y^i(t) . \tag{6}$$

The state $q = 0$ and $q = 1$ correspond respectively to a fully charged and fully discharged battery. The *charging rate* of the battery is given by the time derivative of the total mole fraction.

We assume that lithium can be stored exclusively inside the LFP particles and not elsewhere. Thus in a galvanostatic charging/discharging process the total mole fraction q is the external control parameter. Consequently, the equation (6) represents a constraint on the evolution of the lithium mole fractions $y^1(t), y^2(t), ..., y^{N_\mathrm{P}}(t)$. According to (3) and (6) we have

$$\frac{dq}{dt} = \frac{m_\mathrm{Li}}{k_B T} \sum_{i=1}^{N_\mathrm{P}} \frac{V^i}{V_\mathrm{P}} \frac{1}{\tau^i_\mathrm{Li}} \big(\mu_{s,\mathrm{Li}} - \mu_\mathrm{Li}(y^i)\big) \ . \tag{7}$$

This equation is used to determine the surface chemical potential $\mu_{s,\mathrm{Li}}$. In this context $\mu_{s,\mathrm{Li}}$ may be interpreted as a Lagrange multiplier to satisfy the constraint (6).

Electric current. There is a universal relation between the charging rate dq/dt of the LFP particles and the electric current I which flows through the battery,

$$I = e_0 n_{\mathrm{FePO}_4} V_\mathrm{P} \frac{dq}{dt} \ . \tag{8}$$

Here the physical unit of I is A (Ampere). The relation (8) relies on bulk and surface mass balance equations and will be derived in Section 6.

Battery voltage. The battery voltage U is defined as the electric potential difference between the metal foils of cathode and anode. Based on the constitutive relations of Sect. 6 we obtain the relation

$$U = U^\mathrm{ref} - \tfrac{m_\mathrm{Li}}{e_0} \sum_{i=1}^{N_\mathrm{P}} \tfrac{A^i_\mathrm{E}}{A_\mathrm{E}} \big(\mu_\mathrm{Li}(y^i) - \mu^\mathrm{ref}_\mathrm{Li}\big) - \tfrac{k_B T}{e_0} \Big(\tfrac{1}{A_\mathrm{E} j_\mathrm{P}} + \tfrac{1}{A_\mathtt{A} j_\mathtt{A}} \Big) I. \tag{9}$$

Here j_P and j_A correspond to the total exchange current of the LFP electrode and the lithium anode, respectively. They are defined in terms of the different interfacial dissipative mechanisms happening at the electrodes,

$$\frac{1}{j_\mathrm{P}} = \Big(\frac{1}{j^\mathrm{P}_\mathrm{ic}} + \frac{1}{j^\mathrm{P}_\mathrm{ad}} + \frac{1}{j^\mathrm{P}_\mathrm{re}} \Big) \qquad \text{and} \qquad \frac{1}{j_\mathtt{A}} = \Big(\frac{1}{j^\mathtt{A}_\mathrm{ad}} + \frac{1}{j^\mathtt{A}_\mathrm{de}} \Big) \ . \tag{10}$$

The battery voltage consists of three contributions:

1. The first contribution is a constant voltage $U^\mathrm{ref} = \frac{1}{e_0}(m_{\mathrm{e}^-}\mu_{\mathrm{e}^-}|_{S_\mathtt{C}} + m_{\mathrm{Li}^+}\mu_{\mathrm{Li}^+}|_{S_\mathtt{A}} - m_\mathrm{Li}\mu^\mathrm{ref}_\mathrm{Li})$ which is characterized by the constant chemical potential μ_{e^-} of the electrons at the current collector of the cathode, the chemical potential μ_{Li^+} of lithium of the anode and a reference chemical potential of lithium in iron phosphate.
2. The second contribution depends on the distribution of lithium within the many-particle electrode which is controlled by the equation system (3) and the relation (8).

3. The third contribution is linear in I and takes into account the interfacial dissipative mechanisms. They are characterized by five constant material parameter: lithium intercalation $j_{\mathrm{ic}}^{\mathtt{P}}$, surface reaction $j_{\mathrm{re}}^{\mathtt{P}}$, lithium adsorption at the LFP particles $j_{\mathrm{ad}}^{\mathtt{P}}$, adsorption at the lithium anode $j_{\mathrm{ad}}^{\mathtt{A}}$, and lithium deposition at the anode $j_{\mathrm{de}}^{\mathtt{A}}$. The parameter $j_{\mathrm{ic}}^{\mathtt{P}}$ is related to the intercalation rate k_{Li} by

$$j_{\mathrm{ic}}^{\mathtt{P}} = \tfrac{e_0}{m_{\mathrm{Li}}} k_{\mathrm{Li}} \ . \tag{11}$$

The linearity of the third contribution in the voltage-current relation (9) results from linear relations between fluxes and driving forces. It is easy to extend the model by corresponding nonlinear constitutive equations of Butler-Volmer type [17,18]. In this case we would obtain logarithmic voltage-current relations.

Note that the thermodynamic derivation of Section 6 points out that surface reaction, lithium adsorption and deposition only affect the voltage-current relation (9) but not the dynamics of the many-particle model (3), given by the time dependent amount of lithium distribution within the electrode.

3.2 The stochastic model for the many-particle electrode

In this section we extend the semi-stochastic model of the last paragraph by adding some noise according to the Wiener process. The motivation for that kind of noise will be given at the end of this section.

To introduce noise we assume that the lithium mole fractions $y^1, y^2, ..., y^{N_{\mathtt{P}}}$ represent possible values of a vector-valued random variable $\boldsymbol{Y} = (Y^1, Y^2, ..., Y^{N_{\mathtt{P}}})$.

The set $\{\boldsymbol{Y}(t) |\ t \geq 0\}$ defines a stochastic process that we determine by the SDE system

$$\begin{aligned} Y^i(t) - Y^i(t_0) = &\frac{1}{\tau^i} \frac{m_{\mathrm{Li}}}{k_B T} \int_{t_0}^{t} \big(\mu_{s,\mathrm{Li}}(s) - \mu_{\mathrm{Li}}(Y^i(s))\big)\, ds \\ &+ \nu^i \sqrt{\frac{2}{\tau^i}} \big(W^i(t) - W^i(t_0)\big) - \frac{1}{\tau^i} \big(Z(t) - Z(t_0)\big) \ . \end{aligned} \tag{12}$$

The difference to the semi-stochastic system described above is given by two terms including $W^i(t) - W^i(t_0)$ and $Z(t) - Z(t_0)$, respectively. The first term represents the increment of a Wiener process which models small lithium fluctuations on the surface of the particles. The objects W^i for $i = 1, 2, ..., N_{\mathtt{P}}$ are independent processes. The strength of the noise, ν^i, is controlled by the constant parameter ν_0 which is related to ν^i by

$$\nu^i = \frac{\nu_0}{\sqrt{V^i}} \ . \tag{13}$$

The term $Z(t) - Z(t_0)$ is defined as

$$Z(t) = \frac{\sum_{i=1}^{N_{\mathtt{P}}} \frac{V^i}{V_{\mathtt{P}}} \nu^i \sqrt{\frac{2}{\tau^i}} W^i(t)}{\sum_{j=1}^{N_{\mathtt{P}}} \frac{V^j}{V_{\mathtt{P}} \tau^j}} \ . \tag{14}$$

The function $Z(t)$ is introduced to preserve the constraint (7) for the surface chemical potential $\mu_{s,\mathrm{Li}}$, i.e. $Z(t)$ is introduced such that no noise term appears in the side condition (7). Note that Z is a Gaussian process with covariance $\left(\sum_{i=1}^{N_\mathrm{P}} (\frac{V^i}{V_\mathrm{P}}\nu^i)^2 \frac{2}{\tau^i}\right) / \left(\sum_{j=1}^{N_\mathrm{P}} \frac{V^j}{V_\mathrm{P}\tau^j}\right)^2$, which is infinitesimal for N_P large.

The Wiener process $W = W(t,\omega)$, which is also called Brownian motion, is a particular stochastic process, which is, roughly speaking, a random function of time satisfying (i) its time increments are independent, i.e., for any $r < s < t$, $W(s) - W(r)$ and $W(t) - W(s)$ are independent, (ii) it obeys a Gaussian probability law with mean 0 and variance given by the time increment, i.e. $W(t) - W(s)$ has the law $\mathcal{N}(0, t-s)$. Moreover, the Wiener process is characterized as the process whose distributional time derivative is the *white noise* in one dimension.

Next we give some motivations for the extended stochastic model. At first recall that our previously proposed model in [15] for LFP particles of equal size necessarily needs stochastic fluctuations in order to initiate the observed phase transition. In those papers we introduced the fluctuations to describe the exchange of lithium between the LFP particles during the charging/discharging process, which is the dominate phenomenon for both slow charging rates and equal-size LFP particles. There we ended up with the Fokker Planck equation for the evolution of stored lithium within the many particle electrode. In order to generalize that model for LFP particles of different sizes we propose our semi-stochastic ODE system for N_P particles. Now it is well known that an finite ODE system with a supplemented Wiener process converges to a Fokker Planck equation in the limit $N_\mathrm{P} \to \infty$, see for more details Section 4.1. This is the main reason to introduce the Wiener process in our new ODE system. A more physical point of view is this: One might think that the surface areas of the LFP particles may be randomly covered with imperfections. However, then one has to explain why the influence of the imperfections on the intercalation dynamics is represented by a Wiener process. Thus we prefer to motivate the Wiener process by the limit from the ODE system to the Fokker Planck equation.

The same reasoning can be used to motivate the size dependence of the parameter ν^i because our Fokker Planck setting in [15] unambiguously implies the volume dependence of equation (13).

State of charge. The state of charge q is defined in the same way as for the semi-stochastic model by equation (6). As in the semi-stochastic model, equations (12) and (6) give again (7) for the surface chemical potential $\mu_{s,\mathrm{Li}}$: the terms $W^i(t)$ do not give any explicit contribution in this formula as their sum cancels with the term Z.

Electric current. The relation (8) between the electric current and the total mole fraction is derived from general balance equations without using any constitutive equations. Therefore the relation (8) for the current holds also in the full stochastic setting.

Battery voltage. The derivation of the battery voltage results from the constitutive equation, in particular from the constitutive equation of the lithium flux j_{Li} which depends on the Wiener process. However, we will show in Section 6 that the relation (9) holds also in the stochastic setting.

3.3 Choice of model parameter for LFP electrodes

There are three kinds of distinguished model parameters: energetic, kinetic and structural parameter. Their meaning and values used in the simulation will be now discussed.

Energetic parameter. There are three energetic parameters in the various chemical potentials of the model. The chemical potential μ_{Li} of the LFP particles contains the parameter L representing the heat of solution, which takes into account the interaction of lithium with the iron-phosphate lattice. The parameter L controls the height of the energy barrier between the lithium-rich and the lithium-poor phase. For LFP the parameter L has to be chosen such that the chemical potential μ_{Li} becomes non-monotone allowing phase separation. A typical value for L used in simulation is [1,15,27]

$$L = 94.4 \times 10^{-22}\mathrm{J} \ . \tag{15}$$

A further energetic parameter is the constant reference voltage U^{ref}. Its value depends on the material properties of both the LFP many-particle electrode and the lithium anode. The reference voltage is approximately determined by the mean value of the hysteresis plateaus in a volt-capacity diagram. From Figure 1 we would determine the reference voltage

$$U^{\mathrm{ref}} = 3.4\mathrm{V} \ . \tag{16}$$

The third parameter ν_0 controls the intensity of the fluctuations at the particle surfaces. A suitable value of ν_0 is derived in the Fokker-Planck setting [14],

$$\nu_0 = \sqrt{\frac{k_B T}{L n_{\mathrm{FePO_4}}}} \approx 10^{-14}\mathrm{m}^{\frac{3}{2}} \ . \tag{17}$$

Kinetic parameters. Our constitutive model embodies five distinguished kinetic mechanisms with dissipation. Each mechanism is controlled by a corresponding kinetic coefficient. It is convenient to write the coefficients in the form of exchange currents.

$j_{\mathrm{ic}}^{\mathtt{P}}$	lithium intercalation
$j_{\mathrm{re}}^{\mathtt{P}}$	surface reaction
$j_{\mathrm{ad}}^{\mathtt{P}}$	adsorption at the LFP particles
$j_{\mathrm{ad}}^{\mathtt{A}}$	adsorption at the lithium anode
$j_{\mathrm{de}}^{\mathtt{A}}$	deposition of lithium at the anode .

The kinetic parameters are either determined from atomistic theories or they can be read off from measurements. However, measurements with LFP particles of nano-size are difficult due to the phase transition in LFP. Moreover, the interaction of different surface processes and the experimental handling of composite electrodes bring further complexities.

In particular only a measurement of the total exchange currents $j_{\mathtt{P}}$ and $j_{\mathtt{A}}$ of the cathode and the anode are available in the literature, which appears in our model as the combinations (10) of the kinetic parameter. However, values for $j_{\mathtt{P}}$ differ by several orders of magnitude. Values for $j_{\mathtt{P}}$ in LFP which range from 10^{-6} A m^{-2} to 10^{-1} A m^{-2} are reported [33]. In this study we assume that the rate limiting process in the cathode is the lithium intercalation, i.e both lithium adsorption and electron transfer reaction are fast compared to the intercalation process, i.e.

$$j_{\mathrm{ic}}^{\mathtt{P}} \ll j_{\mathrm{re}}^{\mathtt{P}}, j_{\mathrm{ad}}^{\mathtt{P}} \qquad \Longrightarrow \qquad j_{\mathtt{P}} \approx j_{\mathrm{ic}}^{\mathtt{P}} \ . \tag{18}$$

For the numerical investigations we choose the value

$$j_{\mathrm{ic}}^{\mathtt{P}} \approx j_{\mathtt{P}} = 0.15 \tfrac{\mathrm{A}}{\mathrm{m}^2} \ . \tag{19}$$

According to (11) the kinetic coefficient k_{Li} for the lithium intercalation is

$$k_{\mathrm{Li}} = \tfrac{m_{\mathrm{Li}}}{e_0} j_{\mathrm{ic}}^{\mathtt{P}} = 10^{-8} \tfrac{\mathrm{kg}}{\mathrm{m}^2\mathrm{s}} \ . \tag{20}$$

The exchange current $j_{\mathtt{A}}$ describes lithium ion adsorption and lithium deposition at the anode. Assuming that the surface area of the anode $A_{\mathtt{AE}}$ is large enough, precisely

$$A_{\mathtt{P}} j_{\mathtt{P}} \ll A_{\mathtt{AE}} j_{\mathtt{A}} \ , \tag{21}$$

the adsorption process at the lithium metal electrode has no significant impact on the battery voltage.

According to these assumptions the voltage-current relation (9) for the deterministic model simplifies to

$$U = U^{\mathrm{ref}} - \tfrac{m_{\mathrm{Li}}}{e_0} \sum_{i=1}^{N_{\mathtt{P}}} \tfrac{A_{\mathtt{E}}^i}{A_{\mathtt{E}}} \big(\mu_{\mathrm{Li}}(y^i) - \mu_{\mathrm{Li}}^{\mathrm{ref}}\big) + \tfrac{m_{\mathrm{Li}}}{e_0} \tfrac{k_B T}{e_0} \tfrac{1}{A_{\mathtt{E}} k_{\mathrm{Li}}} I \ . \tag{22}$$

Structural parameters. There are two geometric parameters encoding the specific structure of the LFP electrode, viz.

V^i	the individual volumes of the LFP particles,
$A_{\mathtt{E}}^i$	the individual active surface area of the LFP particles.

The particle volumes can be determine by an analysis of the electrode composition. Fig. 3 depicts a typical particle size distribution from a commercial LFP electrode with spherical particles where the particle volumes can be read off. The particle size distribution defines the probability to find a particle with specific size within the electrode.

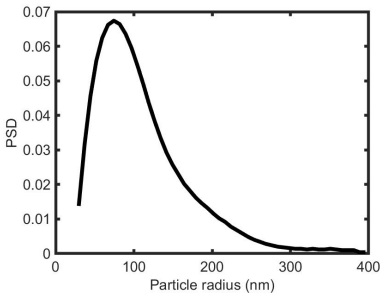

Fig. 3 Typical particle size distribution of a commercial LFP electrode from [41].

The active surface area, more precisely the area where lithium can intercalate into the iron phosphate lattice, cannot be read off from an analysis of the electrode geometry. Coating of the particles as well as the formation of unwanted depositions at particle electrolyte interfaces could be responsible for a decrease of the active surface area. Thus the active surface area might be smaller than the full particle area. Unless otherwise specified, we assume in the simulations that the full particle surface area is the active area and that the particles are spherical, so that the surface areas and the volumes are functions of the particle radii.

4 Various many-particle models in the literature

4.1 The Fokker-Planck setting

It is possible to associate the system of SDEs to a family of Fokker-Planck equations, which give an equivalent description of the SDE system in the limit of large number of particles.

To understand the link between SDEs and Fokker-Planck equations, we start by recalling the following well-known fact: given a drift b, a number σ and a Wiener process W, if a real-valued stochastic process Y satisfies the SDE

$$Y(t) = Y(t_0) + \int_{t_0}^{t} b(s, Y(s))\, ds + \sigma(W(t) - W(t_0)), \tag{23}$$

then, for every $t > 0$, the probability law of Y admits a density $p(t, \cdot)$ which satisfies the Fokker-Planck equation

$$\partial_t p(t, y) = -\partial_y (b(t, y) p(t, x)) + \frac{\sigma^2}{2} \partial_y^2 p(t, y)\ . \tag{24}$$

Now we consider the stochastic model (12) for the many particle electrode in case of single size particles. Note that in this case equation (7) for the surface

chemical potential simplifies to

$$\mu_{s,\mathrm{Li}}(t) = \tau \frac{k_B T}{m_{\mathrm{Li}}} \frac{dq}{dt} + \frac{1}{N_P} \sum_{i=1}^{N_P} \mu_{\mathrm{Li}}(Y^i) \ .$$

where $\tau = \tau^i$ is independent of i. Here we will ignore both the Z term in (12) and the boundary conditions $Y^i \in (0,1)$. We suppose for a moment that the chemical potential $\mu_{s,\mathrm{Li}}$ does not depend on the particle number N_P nor on the specific realization of the noise. Then all particles would be identically distributed, i.e. they have the same probability law, and would behave independently. Then, by the law of large numbers, the system of SDEs (12) with (6) would converge, in a suitable sense, to the single Fokker-Planck equation, viz.

$$\partial_t p(t,y) = \frac{1}{\tau} \frac{m_{\mathrm{Li}}}{k_B T} \partial_y \big((\mu_{\mathrm{Li}}(y) - \mu_{s,\mathrm{Li}}(t)) p(t,y) \big) + \frac{\nu^2}{\tau} \partial_y^2 p(t,y) \ , \tag{25}$$

where $\mu_{s,\mathrm{Li}}$ is given by

$$\mu_{s,\mathrm{Li}}(t) = \tau \frac{k_B T}{m_{\mathrm{Li}}} \frac{dq}{dt} + \int_{-\infty}^{\infty} \mu_{\mathrm{Li}}(y)\, p(t,y)\, dy \ . \tag{26}$$

The main point here for the SDE system (12), and more general for mean field SDEs, is that this convergence remains true, even if the particle are interacting (and so $\mu_{s,\mathrm{Li}}$ is not fixed). This is a classical result, see e.g. [44] for the precise statement. Therefore, in the case of single size particles, this Fokker-Planck equation corresponds to our model in the limit of large number of particles.

The Fokker-Planck equation (25) is identical to the Fokker-Planck equation in [14] for a LFP many particle electrode. In [14] a statistical approach is used to derive the Fokker-Planck equation. Existence and uniqueness of the Fokker-Planck equation in the bounded domain $(0,1)$ is proved in [19]. A detailed discussion of the different time regimes of the Fokker-Planck equation can be found in [29,30]. It is shown in [14] that the Fokker-Planck equation (25) is capable to predict and explain the voltage-capacity diagram and the phase transition within the many particle system. But the Fokker-Planck equation and the model approach of [14] has two import drawbacks: Firstly the Fokker-Planck equation is difficult to extend to systems with different particle sizes and to include phenomena like lithium transport in the LFP particles or electrolyte. Secondly a precise physical interpretation of the parameter τ and ν is missing. Both drawbacks are fully removed by the approach of this paper. In particular, in [14] a Lagrange multiplier Λ was introduced to satisfy the constraint (6) which reads in the Fokker-Planck setting for identical particle sizes

$$q(t) = \int_{-\infty}^{\infty} y\, p(t,y)\, dy \ . \tag{27}$$

The derivation of the SDE system yields that the Lagrange multiplier is the surface chemical potential of lithium, i.e. $\Lambda = \mu_{s,\mathrm{Li}}$. Moreover, in [14] the

coefficient τ was interpreted as the relaxation time of the many particle system, however, dependence on the particle size was missing in [14]. Here we can show that τ is related to the intercalation process of lithium into the iron phosphate lattice and how τ is related to the particle size.

In the case of different size particles, the particles are no more identically distributed, since small particles behave differently from large ones. However, the convergence result remains true, provided we replace the single Fokker-Planck equation (25) by a family of Fokker-Planck equations, parametrized by the radii R of the particles and coupled via the potential $\mu_{s,\mathrm{Li}}$, namely

$$\partial_t p(t,y,R) = \frac{1}{\tau(R)}\frac{m_{\mathrm{Li}}}{k_B T}\partial_y\big((\mu_{\mathrm{Li}}(y)-\mu_{s,\mathrm{Li}})p(t,y,R)\big) + \frac{\nu(R)^2}{\tau(R)}\partial_y^2 p(t,y,R)\ , \tag{28}$$

where now $\mu_{s,\mathrm{Li}}$ is given by

$$\mu_{s,\mathrm{Li}} = \frac{V_{\mathrm{P}}\frac{dq}{dt} + \int\int \mu_{\mathrm{Li}}(y)\,\frac{V(R)}{\tau(R)}\,p(t,y,R)\,dydR}{\int \frac{V(R)}{\tau(R)}\,\rho(R)\,dR}\ , \tag{29}$$

$V(R)$ is the volume of the particle of radius R, and $\tau(R)$ and $\nu(R)$ are suitable functions of the radius. This convergence statement can be shown for example by a randomization procedure, see [24] for a completely analogous proof in the context of Navier-Stokes equations.

The convergence statement for large particle number suggests the stability of simulations (for high enough particle numbers). In practice, we observed stability of simulations for N_P higher than 10^3, therefore the numerical results obtained for $N_P \geq 10^3$ are valid even for higher numbers, in particular for the true number of particles in a LFP electrode (about 10^{17} particles, not feasible to numerical treatment). Simulations for the SDE system with $N_P = 1000$ are fast and easier to implement than for the Fokker-Planck equations, especially in the different size case.

In an upcoming paper we prove rigorously this convergence of the SDE system in presence of boundary conditions [12]. Note indeed that the y^i in (12), being mole fractions, have to live in $[0,1]$ and therefore suitable reflection conditions have to be imposed in (12) when the y^i reach the boundary points 0 or 1.

4.2 Many-particle model for LFP electrodes

In the literature one finds a further remarkable paper dealing with a many-particle models similar to our semi-stochastic model.

The aims of [22] by M. Farkhondeh et al. are the same as in the current study. Farkhondeh et al. propose a dynamical model to describe phase transitions with hysteresis during the charging process of LFP electrodes. Their model consists of the same ingredients of our semi-stochastic model. In our words, Farkhondeh et al. use the same non-monotone chemical potential for

LFP particles as here. They propose a system of relaxation equations for the lithium concentrations of the LFP particles and they impose the constraint that the total electric current of the cell is a weighted sum of the time derivatives of the lithium concentrations, equations (1)-(4) from [22]. The main difference of [22] to our treatment is that Farkhondeh et al. do not recognize that their system of evolution equations (2) and (3) relies on balance equations for the lithium masses of the LFP particles. Thus they must add in the model equations a quite non-physical assumption stating the dependence of the relaxation times on the particle index, equation (5) from [22]. Recall that the balance character of our relation system implies an explicit dependence of the kinetic parameter τ^i of a LFP particle on its volume and effective surface area.

4.3 Many-particle models in the context of atomic chains

Many-particle model are not only limited to the case of many-particle electrodes. Finally we want to mention an interesting paper in the context of atomic chains that uses a third source of stochastic fluctuations.

In [37] A. Mielke and L. Truskinovski study plastic phenomena with phase transition and hysteresis by means of a many-particle model. To this end they consider an atomic chain whose particles interact by bi-stable springs and viscous dashpots. Ignoring the accelerations of the particles, the evolution equations for the mechanical strains have the same form of our evolution system for the stored lithium masses within the LFP particles in our deterministic model. Further correspondences are mechanical stress $\leftrightarrow$ cell voltage, time derivative of the total strain $\leftrightarrow$ electric current in the electrode model, and elastic part of the particle forces $\leftrightarrow$ non-monotone chemical potentials of the LFP particles. The two phenomenological parameters of our evolution system also appears in [37], but in contrast to our treatment the parameters are assumed to be independent of the particular particle of the atomic chain. Obviously Mielke and Truskinovski also observed that such a model is not capable to describe phase transitions with hysteresis. In order to embody that phenomenon they introduce a distribution of reference forces over the particles of the chain which would correspond to a distribution of the reference values of the chemical potentials in our many particle model for the electrode. However, it is known that the reference value of the chemical potentials is the same for all LFP particles. Thus from a physical point of view we find it more natural to introduce a distribution of different relaxation parameter which would correspond to a distribution of viscosities in [37].

5 Behavior of the many-particle model

In this section we show some selected results of numerical simulations of the LFP electrode model. We study the influence of (i) charging time, (ii) stochastic noise, (iii) particle size distribution and (iv) active surface areas on the

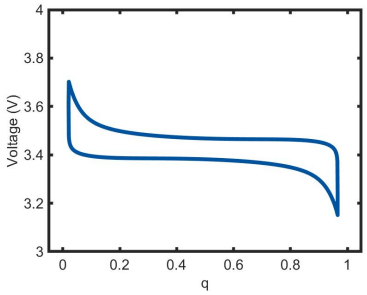

Fig. 4 Symmetric voltage hysteresis of a charge-discharge processe for a 1C charging rate.

dynamics of the SDE system. Here we distinguish between the influence on the microscopic behavior of the system, i.e. the behavior of individual storage particles, and on the macroscopic behavior, i.e. the battery voltage U.

For the simulations we assume spherical particles and we denote the particle radius of particle P^i with R^i. We use a particle size distribution of a commercial LFP electrode which serves as reference distribution [41], Figure 3. Further distributions are generated by stretching and shifting of the reference distribution. To compare a particle size distribution and a particle system with identical particles, we keep the same number of particles and we choose the size of the identical particles in such a way that the total particle volumes of both systems are equal.

An analysis of the SDE system shows that a solution $(Y_i^{\text{charge}})_{i=1,\dots,N}$ of a charging process with q_{charge} can be used to define a solution of discharge process by $(Y_i^{\text{discharge}})_{i=1,\dots,N}$ and $q_{\text{discharge}} = 1 - q_{\text{charge}}$ due to the symmetric chemical potential (5). Therefore a simulation of charge and discharge processes with the same charging rate is symmetric. In Figure 4 a symmetric voltage hysteresis for a 1C charging process is shown. Due to this symmetry we only consider discharge curves to illustrate the behavior of the many-particle model.

The following simulations are done with approximately 5000 particles. This value provides feasible and stable simulations, see the end of Section 4.1. We replace the surface chemical potential $\mu_{s,\text{Li}}$ in the SDE system (12) by the relation (7) and we obtain an SDE system for the mole fractions Y_i. All simulations have been implemented in MATLAB and performed with an explicit Euler scheme with fixed time step size. The simulations are stopped when one concentration Y^i reaches 0 or 1 as consequence of noise or numerical error.

Impact of the particle size distribution. At first we study the differences between single size and different size cases on the macroscopic behavior of the many-particle electrode model, for different charging rates and in precence of stochastic fluctuations.

To allow a better comparison of the simulations with different charging rates, we ignore the linear shift in the representation for the battery voltage

(9). Then the voltage of the battery is defined by the (dimensionless) mean chemical potential $\langle \mu_{\mathrm{Li}} \rangle$,

$$\langle \mu_{\mathrm{Li}} \rangle(t) \;=\; \tfrac{m_{\mathrm{Li}}}{k_B T} \sum_{i=1}^{N_{\mathrm{P}}} \tfrac{A_{\mathrm{E}}^i}{A_{\mathrm{E}}} (\mu_{\mathrm{Li}}(Y^i(t)) - \mu_{\mathrm{Li}}^{\mathrm{ref}}) \; . \tag{30}$$

In Figure 5 the mean chemical potential $\langle \mu_{\mathrm{Li}} \rangle$ against the state of charge q is plotted. In the case of single size particles the simulations show strong oscillations and a non-monotone behavior in the $\langle \mu_{\mathrm{Li}} \rangle$-$q$ plot. Only for the extreme slow charging rate C/20000 the simulation with the single size particles shows the typical horizontal voltage plateau of LFP electrodes. On the other hand all simulations with the particle size distribution of Figure 3 exhibit flat plateaus and show bare oscillations.

From this observation we conclude that the many-particle model with single size particles is only capable to predict experimental observed voltage plateaus for very slow charging rates. On the contrary the many-particle model with particle size distribution predicts the voltage plateaus in all charging regimes.

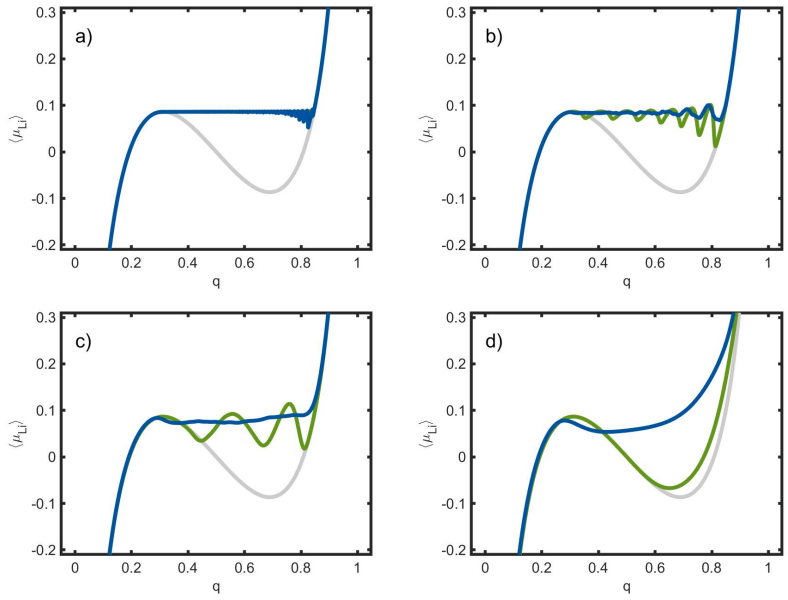

Fig. 5 Comparison of simulations with particles of the same size and size distribution. Mean chemical potential $\langle \mu \rangle$ over state of charge q for single size particles (green) and particle size distribution (blue). The gray curve indicates the chemical potential $\mu_{\mathrm{Li}} - \mu_{\mathrm{Li}}^{\mathrm{ref}}$. Charging rate: a) C/20000, b) C/500, c) C/100, d) C/25.

Impact of stochastic fluctuations. Next we study the impact of the stochastic fluctuations on the macroscopic behavior of the many-particle model.

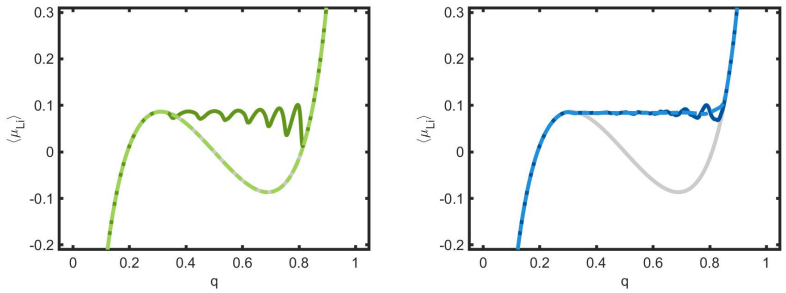

Fig. 6 Impact of the stochastic fluctuations on the mean chemical potential $\langle \mu_{\mathrm{Li}} \rangle$. Left: Single size particles without (dashed) and with stochastic fluctuations (solid), Right: Particle size distribution without (dashed) and with stochastic (solid). Charging rate C/500. The gray curve indicates the chemical potential $\mu_{\mathrm{Li}} - \mu_{\mathrm{Li}}^{\mathrm{ref}}$.

Figure 6 shows the simulations with and without stochastic fluctuation for both electrodes with single size particles and particle size distributions for the charging rate C/500.

We observe for the simulation with single size particles and without fluctuation that the horizontal voltage plateau vanishes and the mean chemical potential follows the non-monotone curve of the chemical potential of a single particle. Conversely, the simulation with particle size distribution shows nearly no observable influence of the stochastic fluctuations on the mean chemical potential, i.e. on the battery voltage.

We conclude that the model with single size particles and without stochastic fluctuations is not capable to predict the horizontal voltage plateaus even in a slow charging regime. In the case with particle size distribution the the stochastic fluctuations have a minor impact on the battery voltage and the horizontal voltage plateau is preserved.

Phase separation. To illustrate the phase separation within the electrode during a discharging electrode, we consider snapshots of the lithium distribution within the electrode for half-discharged electrodes, i.e. $q = 0.5$.

We start with simulations in the slow charging regime of C/500 with stochastic fluctuations. Figure 7 shows the corresponding snapshots of the particle mole fractions at $q = 0.5$. Here the simulations with single size particles and particle size distribution as well exhibit a pronounced phase separation. Almost all particles are either in the lithium rich phase or in the lithium poor phase.

The simulation with particle size distribution further shows that small particles undergo the phase transition first while larger particles exhibit the phase transition later. However, Figure 7_{right} likewise shows that the phase transition do not exclusively depend on the particle size.There exist a broad region where small and large particles coexist in the same phase. Furthermore the simulation shows that several large particles remain in an intermediate phase even for a macroscopic time period, i.e. these particles are neither in the

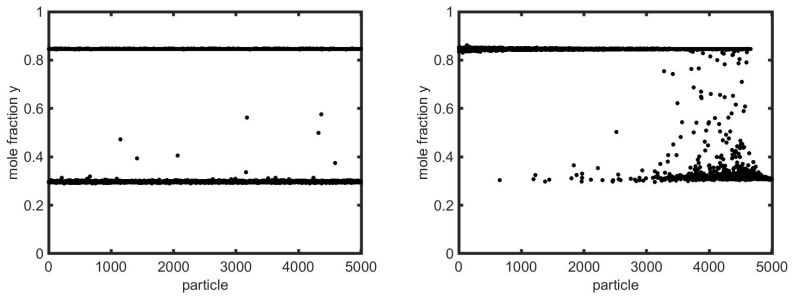

Fig. 7 Impact of the particle size distribution on the phase separation at charging rate 1/500 C. Particles are ordered by size. Simulations with stochastic fluctuation. Mole fraction y of the individual storage particles at the state $q = 0.5$. Left: single size particles, Right: particle size distribution.

lithium rich nor in the lithium poor phase. These findings are in agreement with experiments on LFP electrodes [34,33,8].

In the charging regime C/500 with single size particles, but without stochastic fluctuations, the behavior drastically changes. All particles behave identically and no phase separation is observable anymore, Figure 8_{left}. This explains the behavior observed in Figure 5 where the mean chemical potential follows the non-monotone curve of the chemical potential of a single particle.

Conversely, for the many particle model with particle size distribution, but without surface fluctuations, a two-phase system is established. Due to the missing stochastic fluctuations the set in of the phase transition is ordered by the particle size, as it is depicted in Figure 8_{right}.

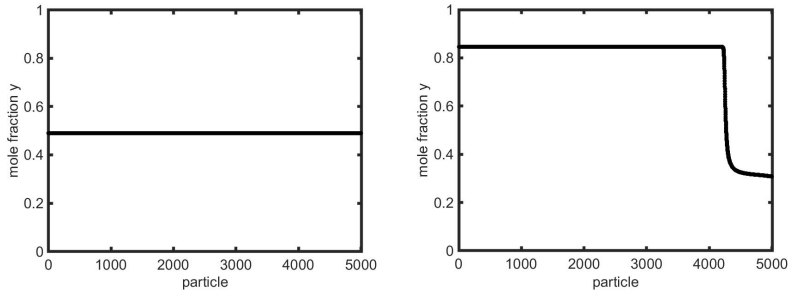

Fig. 8 Impact of the particle size distribution on the phase separation at charging rate 1/500 C. Particles ordered by size. Simulations without stochastic fluctuations. Mole fractions y of the individual storage particles at the state $q = 0.5$. Left: single size particles, Right: particle size distribution.

We consider now the fast charging regime 1C. In the single size case there is, even under the influence of surface fluctuations, no phase separation in the particle system and all particle behave identically as it is depicted for $q = 0.5$ in Figure 9_{left}. This also explains the behavior of the mean chemical potential in

Figure $(5)_{\mathrm{d})}$ where the potential follows the non-monotone chemical potential of a single particle. In case of the particle size distribution only small particles reach a lithium rich phase at $q = 0.5$, while the larger particles remain in an intermediate phase, Figure 9_{right}. As before in the slow charging regime the order of particles undergoing a phase transition depends on the particle size.

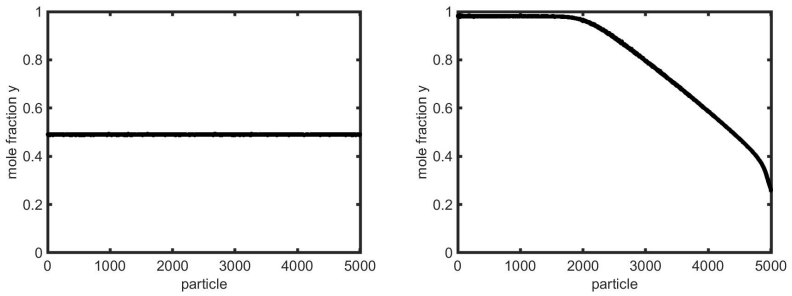

Fig. 9 Impact of the particle size distribution on the phase separation at charging rate 1 C. Simulations with stochastic fluctuation. Mole fraction y of the individual storage particle at the state $q = 0.5$. Left: single size particles, Right: particle size distribution (particles ordered by size).

To summarize, both the particle size distribution and the stochastic fluctuations have an impact on the microscopic dynamics of the SDE systems, particularly on the phase separation.

In the case of single size particles only simulations with stochastic fluctuation and for slow charging rates predict a phase separation. In simulations without fluctuations or for high charging rates all particles behave identically and a phase separation is missing.

All simulations with particle size distribution show phase separation within the electrode even in the case without stochastic fluctuations. The simulations also predict a dependence of the phase transition on the particle size. This finding is experimentally observed in LFP electrodes where the electric conduction is improved by addition of carbon black [34]. Furthermore the simulations show that larger particles seem to prefer an intermediate state and this behavior is even stronger pronounced for high charging rates. Likewise this finding is in agreement with experiments. Chueh et al. show that in LFP electrodes with small ellipsoidal particles of mean size 230nm two coexisting phases exist whereas electrodes with large platelet particles of mean size 3μm are homogeneous and they are simultaneously filled [35].

Various particle size distribution. Next we study the effects of different particle size distributions on the battery voltage. As discussed above the surface fluctuations have no effect the battery voltage for the particle size distribution form Figure. 3. Therefore we have been performed all simulations without stochastic fluctuations. We exclusively consider the fast charging regime 1C.

We start with the reference particle size distribution from Figure 3. To generate new size distributions the original distribution ranging from 25nm up to 400nm is now stretched and shifted, respectively. Figure 10 depicts three discharging processes with rate 1C for increasingly stretched size distributions. Both the height of the voltage plateau and the value of q where a sharp drop of the voltage occurs, decrease for increasingly stretched size distributions, i.e. the size distribution has a pronounced effect on the rate dependent capacity of the battery.

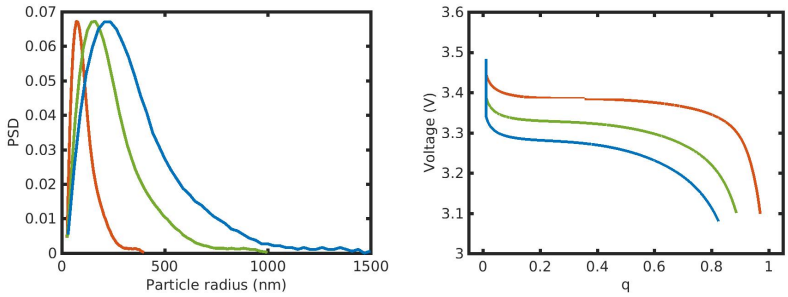

Fig. 10 Impact of stretched size distribution: $25-400nm$ (red), $25-1000nm$ (green), $25-1500nm$ (blue); Left: particle size distributions, Right: corresponding voltage for a discharge process at rate 1C.

In Figure 11 the reference size distribution is shifted by fixed values. Here the voltage decreases as the distribution is shifted to bigger sized particles but the rate dependent capacity remains the same. This is in contrast to real batteries where a reduction of the rate dependent capacity would be expected. The origin of this deficiency might be the assumption of fast diffusion within the LFP particles, which is not satisfied for particle size distribution in the micrometer range. However, this assumption is necessary in order to handle homogeneous particles only. Note that these observation is crucial for more detailed studies on the effects of particle size distributions on the performance of batteries.

Impact of the active area. A crucial parameter in our model is the active area A^i_{E}, which is the area of particle P^i where lithium can intercalate. In batteries this active area depends on the ionic and electronic conductivity of the particle to both electrode and electrolyte. Manufacturing processes as surface coating may affect the active area [38].

To us it seems reasonable that small particles have a larger ratio of active area to the full particle surface area as large particles. Figure 12_{left} shows three different ratios of active area-particle surface area that are used in the simulations shown in Figure 12_{right}. The active areas are calculated by the interpolation formula $A^i_{\mathrm{E}} = 4\pi(R_i)^2(\frac{1}{2}(1-(R_i-R_{\min})/(R_{\max}-R_{\min}))^x + (1-x))$, where x is the desired ratio of active area-particle surface area of

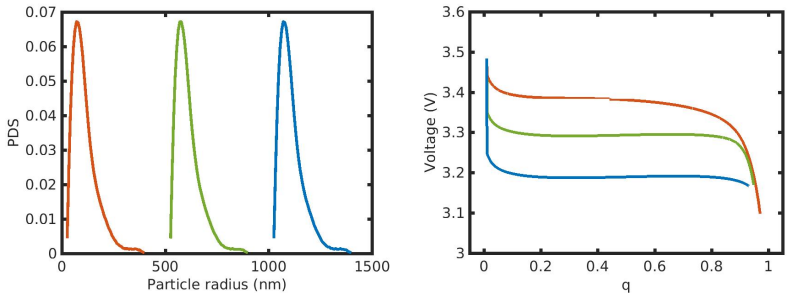

Fig. 11 Impact of shifted size distribution: $25-400nm$ (red), $525-900nm$ (green), $1025-1400nm$ (blue); Left: particle size distributions, Right: corresponding voltage for discharge process with rate 1C.

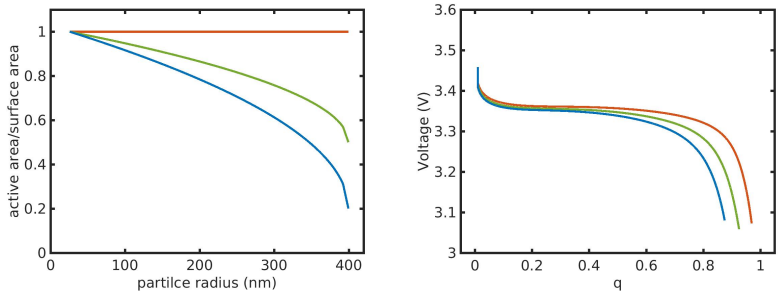

Fig. 12 Impact of active surface areas. Left: ratio between active surface area and total surface area. Right: corresponding voltage for 1C discharge process.

the larges particle and $R_{\min}$ and $R_{\max}$ are the radii of the smallest and larges particle respectively.

The effect of the active area on the battery voltage is shown for a discharge process with rate 1C. For the simulations the surface fluctuations are not taken into account. The simulation shows that reducing the active area according to Figure $(12)_{\text{left}}$ reduces the rate dependent capacity.

Impact of the charging rate and fit to the experiments. For the comparison with experiments we use the data from [41]. The particle size distribution of the battery studied in [41] corresponds to the reference distribution of Figure 3. Figure 13 shows a comparison of experimental and simulated voltage-capacity curves for the charging rates C/25, 1C and 3C. The simulations are performed without surface fluctuations, since their impact on the voltage is marginal as discussed above. The active area used for this simulation corresponds to the green curve in Figure 12_{left}.

An increase of the charging rates reduces the rate dependent capacity. Moreover, the height of the voltage plateau decreases for higher charging rates. This is in good agreement with the experimental data. Although the many-particle model is quite simple, with only two constant kinetic parameters,

we observe good matches between simulations and experiments for slow and moderate charging rates. Only for the fast charging rate 3C the simulation shows some deviation from the measurement. This deviation might be due to diffusion processes within the electrode particles or electrolyte, which are not taken into account in the many-particle model.

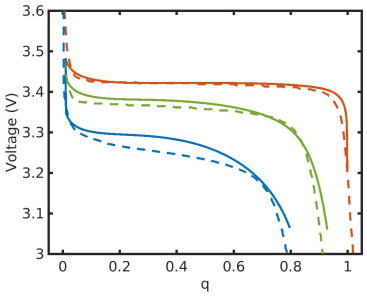

Fig. 13 Comparison between simulation and experiment for different charging rates: C/25 (red), 1C (green), 3C (blue). Solid line – simulation, dashed line – experiment. Experimental data taken from [41]

6 Thermodynamic model of a many-particle electrode and its coupling to the surrounding

In this section both the SDE system and the cell voltage- current relation will be derived on a thermodynamic basis. In a first step we describe an electrochemical system in a general thermodynamic framework. The model equations are grouped into two different classes: i) universal equations of balance for mass, momentum, energy and entropy and Maxwells equations and ii) constitutive equations that describe the special material properties of the system at hand.

We restrict ourselves to a non-viscous, isothermal, non-polarizable and non-magnetizable systems where accelerations and the magnetic field can be ignored, i.e. the temperature is assumed to be constant, the quasi-static version of the momentum balance and the electrostatic approximation of Maxwells equations are applicable.

Here we present only a brief introduction of the thermodynamic framework, which is absolutely necessary to understand the derivation of the LFP electrode model. A detailed description of non-equilibrium thermodynamics and its coupling to electrodynamics can be found in [36, 7, 3, 39, 26].

6.1 General thermodynamic setting

In the general setup we consider an arbitrary domain Ω that is separated by a surface S into two subdomains $\Omega^{\pm}$ so that $S = \partial\Omega^{+} \cap \partial\Omega^{-}$. In order to indicate whether a generic quantity u is defined in the bulk domains $\Omega^{\pm}$ or on the surface S we write $u^{\pm}$ and u_s, respectively.

A point on S is equipped with a surface normal $\boldsymbol{\nu}$ pointing by convention into the domain Ω^{+}.

The boundary ∂S of S is assumed to be a closed line on S that is characterized by a unit vector $\boldsymbol{e}$ lying tangential to S and normal to ∂S.

Constituents and basic quantities. Within the domains $\Omega^{\pm}$ and on the surface S we have general mixtures consisting of $(N^{\pm}+1)$ and (N_s+1) constituents, which are denoted by $A_0, A_1, ..., A_{N^{\pm}}$ and $A_{s,0}, A_{s,1}, ..., A_{s,N_s}$. Each constituent of $\Omega^{\pm}$ is also present on S, but here there may be additional constituents that are exclusively present on S, i.e. $N^{+} + N^{-} \leq N_s$. The set of constituents of the bulk domains and of the surface are denoted by $\mathcal{M}^{\pm}$ and $\mathcal{M}_s$, respectively. Further we assume that the constituents of the bulk domains are different, i.e. $\mathcal{M}^{+} \cap \mathcal{M}^{-} = \emptyset$. In case of identical chemical species in both bulk domains, we treat these species as different constituents. This is reasonable and necessary because a constituent may have different physical and chemical properties in the domains $\Omega^{\pm}$.

The general thermodynamic setting is the same for both domains $\Omega^{\pm}$. Thus for a simplified notation we omit the superscripts $\pm$ and indicate the corresponding domains only if necessary.

The constituent A_0 plays a special role. For example, in an liquid electrolyte A_0 indicates the solvent and in solid electrode A_0 represents the constituent forming the crystal lattice.

In the isothermal and electrostatic setting the thermodynamic state of the bulk mixture is characterized by the number densities $(n_\alpha)_{\alpha\in\mathcal{M}^{\pm}}$, the barycentric velocity $\boldsymbol{v}$ and the electric potential φ. On the surface the thermodynamic state is given by the surface number densities $(n_{s,\alpha})_{\alpha\in\mathcal{M}_s}$, the barycentric surface velocity $\boldsymbol{v}_s$ and the surface electric potential φ_s. These variables may be functions of time and space.

Each constituent A_α of the bulk or surface has the atomic mass m_α and may be carrier of charge $z_\alpha e_0$, where z_α is the charge number and e_0 is the elementary charge.

Among the surface constituents we may have M_s surface chemical reactions of the general form

$$\mathrm{a}^{\mathrm{i}}_0\mathrm{A}_{\mathrm{s},0} + \cdots + \mathrm{a}^{\mathrm{i}}_{\mathrm{n_s}}\mathrm{A}_{\mathrm{s},\mathrm{N_s}} \underset{R^i_{s,b}}{\overset{R^i_{s,f}}{\rightleftharpoons}} \mathrm{b}^{\mathrm{i}}_0\mathrm{A}_{\mathrm{s},0} + \cdots + \mathrm{b}^{\mathrm{i}}_{\mathrm{N_s}}\mathrm{A}_{\mathrm{s},\mathrm{N_s}} \qquad \text{for i} \in \{1, \cdots, M_s\} \ . \tag{31}$$

The constants a^i_α, b^i_α are positive integers and $\gamma^i_\alpha = b^i_\alpha - a^i_\alpha$ denote the stoichiometric coefficients of the reaction i. $R^i_{s,f}$ and $R^i_{s,b}$ denote the forward

and backward reaction rates, respectively. The net reaction rate is defined as $R_s^i = R_{s,f}^i - R_{s,b}^i$.

Multiplication of the number densities n_α by the masses m_α gives the partial mass densities in the bulk and on the surface:

$$\rho_\alpha = m_\alpha n_\alpha \qquad \text{and} \qquad \rho_{s,\alpha} = m_\alpha n_{s,\alpha} \ . \tag{32}$$

For the bulk and surface mixture, the mass densities are defined by

$$\rho = \sum_{\alpha=0}^{N} \rho_\alpha \qquad \text{and} \qquad \rho_s = \sum_{\alpha=0}^{N_s} \rho_{s,\alpha} \ . \tag{33}$$

Finally, the free charge densities are defined by

$$n^{\mathrm{F}} = \sum_{\alpha=0}^{N} z_\alpha e_0 n_\alpha \qquad \text{and} \qquad n_s^{\mathrm{F}} = \sum_{\alpha=0}^{N_s} z_\alpha e_0 n_{s,\alpha} \ . \tag{34}$$

Jumps at the surface. We introduce the boundary values, the jump and the mean value of a generic bulk function $u(t,x) \in \Omega^\pm$ at S as

$$u|_S^\pm = \lim_{x \in \Omega^\pm \to S} u \qquad \text{and} \qquad [\![u]\!] = u|_S^+ - u|_S^- \qquad \text{and} \qquad \langle u \rangle = \tfrac{1}{2}(u|_S^+ + u|_S^-) \ . \tag{35}$$

In case that the function u is not defined in Ω^+ or in Ω^-, the corresponding value in (35) is set equal to zero.

6.2 Balance of mass and momentum

Customarily non-equilibrium thermodynamics uses the local equations of balance. However, for the derivation of the SDE system it is convenient to use the global version of the mass balances, i.e. in terms of integrals. On the other hand, the momentum balances, Maxwell's equations and the constitutive equations are still represented by their local forms.

Bulk mass balance. The determination of the mass densities $\rho_\alpha = m_\alpha n_\alpha$ relies on the balance equations of mass. The mass of constituent A_α, $\alpha = 0, 1, ..., N$, changes due to convection, diffusion and chemical reactions,

$$\frac{d}{dt}\int_\Omega m_\alpha n_\alpha \, dx = -\int_{\partial\Omega} \boldsymbol{j}_\alpha \cdot \boldsymbol{\nu} \, da + \int_\Omega r_\alpha \, dx \qquad \text{with} \quad \boldsymbol{j}_\alpha = \rho_\alpha(\boldsymbol{v} - \boldsymbol{w}) + \boldsymbol{J}_\alpha \ . \tag{36}$$

The quantities r_α are the mass production densities. Here we do not consider chemical reactions in the bulk domains, i.e. we have $r_\alpha = 0$. The velocity of the boundary $\partial\Omega$ is denoted by $\boldsymbol{w}$ and $\boldsymbol{J}_\alpha$ is the bulk diffusion flux of constituent A_α. To guarantee the total mass conservation the diffusion fluxes satisfy the side condition [36,7,39]

$$\sum_{\alpha=0}^{N} \boldsymbol{J}_\alpha = 0 \ . \tag{37}$$

Surface mass balance. The surface mass density $\rho_{s,\alpha} = m_\alpha n_{s,\alpha}$, of the surface constituent $A_{s,\alpha}$ is determined by surface mass balance equation,

$$\frac{d}{dt}\int_S m_\alpha n_{s,\alpha}\,da = -\int_{\partial S} \boldsymbol{j}_{s,\alpha}\cdot \boldsymbol{e}\,dl - \int_S [\![\boldsymbol{j}_\alpha\cdot\boldsymbol{\nu}]\!]\,da + \int_S r_{s,\alpha}\,da. \tag{38}$$

The line integral gives the tangential mass flux normal to the line ∂S into the surface S, while the normal flux from the bulk domains across the surface S is represented by the double bracket. The tangential mass flux density is denoted by $\boldsymbol{j}_{s,\alpha}$ and consists of convection and diffusion,

$$\boldsymbol{j}_{s,\alpha} = \rho_{s,\alpha}(\boldsymbol{v}_{\tau,s} - \boldsymbol{w}_\tau) + \boldsymbol{J}_{s,\alpha}\ , \tag{39}$$

where $\boldsymbol{v}_{\tau,s}$ and $\boldsymbol{w}_\tau$ represent the tangential parts of the surface barycentric velocity $\boldsymbol{v}_s$ and of the surface velocity $\boldsymbol{w}$ of S, respectively. The tangential diffusion flux of constituent $A_{s,\alpha}$ on S is denoted by $\boldsymbol{J}_{s,\alpha}$. As in the bulk the diffusion fluxes must satisfy the side condition

$$\sum_{\alpha=0}^{N_s} \boldsymbol{J}_{s,\alpha} = 0\ . \tag{40}$$

The third term on the right hand side of (38) represents surface chemical reactions with surface mass production densities $r_{s,\alpha}$. The production densities are related to the reaction rates by

$$r_{s,\alpha} = \sum_{i=1}^{M_s} \gamma_{s,\alpha}^i m_\alpha R_s^i\ . \tag{41}$$

Bulk momentum balance. In the quasi-static setting the Cauchy stress $\boldsymbol{\sigma}$ of the matter is balanced by the electrostatic force $-n^{\mathrm{F}}\nabla\varphi$,

$$-\mathrm{div}(\boldsymbol{\sigma}) = -n^{\mathrm{F}}\nabla\varphi \qquad \text{in } \Omega\ . \tag{42}$$

Here the force density due to gravitation is ignored. An alternative formulation of the momentum balance reads, [39,16],

$$\mathrm{div}\boldsymbol{\Sigma} = 0 \qquad \text{in } \Omega\ , \tag{43}$$

where the newly introduced quantity $\boldsymbol{\Sigma}$ is the total stress tensor,

$$\boldsymbol{\Sigma} = \boldsymbol{\sigma} + \varepsilon_0\big(\nabla\varphi\otimes\nabla\varphi - \tfrac{1}{2}|\nabla\varphi|^2\mathbf{1}\big)\ . \tag{44}$$

Surface momentum balance. The quasi-static surface momentum balance equation is represented by, [39,6],

$$[\![\boldsymbol{\Sigma}\cdot\nu]\!] = -2k_M\gamma_s\boldsymbol{\nu} - \nabla_s\gamma_s \qquad \text{on } S\ , \tag{45}$$

where γ_s denotes the surface tension and k_M is the mean curvature of the surface S.

6.3 Maxwells equations and electric current

In the quasi-static regime Maxwells equations are significantly reduced. The equations for the electric field $\boldsymbol{E}$ can be solved by introducingan electric potential φ,

$$\boldsymbol{E} = -\nabla\varphi \ . \tag{46}$$

Without polarization the solely relevant Maxwell equation in the bulk is the Poisson equation,

$$\operatorname{div}(\varepsilon_0 \boldsymbol{E}) = n^{\mathrm{F}} \ . \tag{47}$$

The quantity ε_0 is the dielectric constant. Maxwells equations for the surface S separating the bulk domains $\Omega^{\pm}$ are satisfied by (i) a continuous electric potential,

$$\varphi_s = \varphi|_S^+ = \varphi|_S^- \tag{48}$$

and (ii) by the jump condition for the electric field

$$[\![\varepsilon_0 \boldsymbol{E}]\!] \cdot \boldsymbol{\nu} = n_s^{\mathrm{F}} \ . \tag{49}$$

A further crucial equation in electrochemical systems is the electric charge balance,

$$\frac{d}{dt}\int_\Omega n^{\mathrm{e}} dx = -\int_{\partial\Omega} \boldsymbol{j}^{\mathrm{e}} \cdot \boldsymbol{\nu}\, da \quad \text{with} \quad \boldsymbol{j}^{\mathrm{e}} = n^{\mathrm{e}}(\boldsymbol{v} - \boldsymbol{w}) + \boldsymbol{J}^{\mathrm{e}} \ . \tag{50}$$

where n^{e} is the electric charge density and $\boldsymbol{J}^{\mathrm{e}}$ is the electric current density. In a non-polarizable and non-magnetizable system charge density and electric current density are represented by

$$n^{\mathrm{e}} = n^{\mathrm{F}} \qquad \text{and} \qquad \boldsymbol{J}^{\mathrm{e}} = \sum_{\alpha=0}^{N} \tfrac{z_\alpha e_0}{m_\alpha} \boldsymbol{J}_\alpha \ , \tag{51}$$

i.e. they are determined by the number densities and the diffusion fluxes of the constituents. For the surface S the corresponding charge balance reads

$$\frac{d}{dt}\int_S n_s^{\mathrm{e}}\, da = -\int_{\partial S} \boldsymbol{j}_s^{\mathrm{e}} \cdot \boldsymbol{e}\, dl - \int_S [\![\boldsymbol{j}^{\mathrm{e}} \cdot \boldsymbol{\nu}]\!]\, da \qquad \text{with} \qquad \boldsymbol{j}_s^{\mathrm{e}} = n_s^{\mathrm{e}}(\boldsymbol{v}_{\tau,s} - \boldsymbol{w}_\tau) + \boldsymbol{J}_s^{\mathrm{e}} \ . \tag{52}$$

In an analogous manner to the bulk the surface electric charge density n_s^{e} and the surface electric current density $\boldsymbol{J}_s^{\mathrm{e}}$ are given in a non-polarizable and non-magnetizable system by

$$n_s^{\mathrm{e}} = n_s^{\mathrm{F}} \qquad \text{and} \qquad \boldsymbol{J}_s^{\mathrm{e}} = \sum_{\alpha=0}^{N_s} \tfrac{z_\alpha e_0}{m_\alpha} \boldsymbol{J}_{s,\alpha} \ . \tag{53}$$

6.4 Constitutive model

The balance equations for mass and momentum have to be supplemented by constitutive equations for the mass fluxes $\boldsymbol{J}_\alpha$, $\boldsymbol{J}_{s,\alpha}$ and for the surface reaction rates R_s^i. The constitutive equations are restricted by the principle of material objectivity and the 2$^{\text{nd}}$ law of thermodynamics consisting of a list of axioms. In the following most results are derived in [7,3,4,26].

Free energy, chemical potentials and electrochemical potentials. The crucial quantities of a constitutive model are the free energy functions for bulk and surface materials. The free energy functions must be given at first. Then all other constitutive quantities can be represented by the free energy functions and their derivatives in a thermodynamically consistent manner. For the different mixtures of the current study we use free energy functions of the general form

$$\rho\psi = \rho\psi(T, \rho_0, \dots, \rho_N) \qquad \text{and} \qquad \rho_s\psi_s = \rho_s\psi_s(T_s, \rho_{s,0}, \dots, \rho_{s,N_S}) \ . \quad (54)$$

Note that in non-polarizable and non-magnetizable materials, the free energy functions do not explicitly depend on the electromagnetic fields. The interested reader might consult [39,17,26] where more details on polarization and magnetization can be found. In the isothermal setting surface temperature T_s and bulk temperature T are constant and equal in each phase. Therefore the temperature occurs here only as a constant parameter.

The chemical potentials of bulk and surface materials are defined by

$$\mu_\alpha = \frac{\partial\rho\psi}{\partial\rho_\alpha} \qquad \text{and} \qquad \mu_{s,\alpha} = \frac{\partial\rho_s\psi_s}{\partial\rho_{s,\alpha}} \ . \quad (55)$$

In addition to the chemical potentials there are electrochemical potentials which play the central role in the constitutive equations, particularly in the isothermal case. The electrochemical potentials are defined by

$$\mu_\alpha^e = \mu_\alpha + \tfrac{z_\alpha e_0}{m_\alpha}\varphi \qquad \text{and} \qquad \mu_{s,\alpha}^e = \mu_{s,\alpha} + \tfrac{z_\alpha e_0}{m_\alpha}\varphi_s \ . \quad (56)$$

Diffusion fluxes for the bulk domains. The $N+1$ diffusion fluxes $\boldsymbol{J}_\alpha$ must satisfy the side condition (37) so that only N constitutive equations can be given. In the isothermal setting the 2nd law of thermodynamics is guaranteed by the choice [7]

$$\boldsymbol{J}_\alpha = -M_\alpha\nabla(\mu_\alpha^e - \mu_0^e) \ , \quad \alpha = 1, \cdots, N \ . \quad (57)$$

The mobility coefficients $M_\alpha > 0$ are non-negative material parameters.

Cauchy stress tensor and pressure. For simplicity, we assume that the viscosity has a minor impact on the battery performance and can be neglected. Then the simplest thermodynamically consistent constitutive equation for the Cauchy stress tensor reads

$$\boldsymbol{\sigma} = -p\mathbf{1} \ , \tag{58}$$

where p is the material pressure satisfying the Gibbs-Duhem equation

$$p = -\rho\psi + \sum_{\alpha=0}^{N} \rho_\alpha \mu_\alpha \ . \tag{59}$$

Diffusion fluxes for the surface S. The equations of surface mass balances (38) have to be supplemented by constitutive equations for the tangential diffusion fluxes $\boldsymbol{J}_{s,\alpha}$ and the normal components of the mass fluxes $\boldsymbol{j}_\alpha$. As in the volume the surface constitutive relations are related to the surface electrochemical potentials. We choose the following thermodynamically consistent constitutive equations for the mass fluxes, [3,26],

$$\boldsymbol{J}_{s,\alpha} = -M_{s,\alpha}\nabla_s(\mu^e_{s,\alpha} - \mu^e_{s,0}) \ , \quad \alpha = 1, \cdots, N_s \ , \tag{60a}$$

$$\boldsymbol{j}_\alpha \cdot \boldsymbol{\nu}|_S^\pm = \mp M^\pm_{s,\alpha}\big((\mu^e_\alpha - \mu^e_0)|_S^\pm - (\mu^e_{s,\alpha} - \mu^e_{s,0})\big) \ , \quad \alpha = 1, \cdots, N^\pm \ , \tag{60b}$$

$$\rho(\boldsymbol{v} - \boldsymbol{w}) \cdot \boldsymbol{\nu}|_S^\pm = \mp L_s^\pm(\mu^e_0|_S^\pm - \mu^e_{s,0} \pm f^\pm) \ , \tag{60c}$$

where $M_{s,\alpha}$, $L_s^\pm$ and $M^\pm_{s,\alpha}$ denote non-negative material parameter, the so called kinetic coefficients. These constitutive equations embody surface diffusion, (60a), and adsorption from the bulk to the surface S, (60b) and (60c). The newly introduced quantities $f^\pm$ will be used to model stochastic processes on the particle surfaces in Section 6.9 .

Note that the surface constitutive equations (60b) and (60c) depend on the constitutive assumptions that were made for the bulks, [3,26]. For example, if we were to consider a viscous material so that viscous term occurs in the constitutive equation for the Cauchy stress (58), then additional viscous terms would likewise arise in the constitutive equation (60c).

Surface tension. The constitutive equation for the surface tension is similar to the Gibbs-Duhem equation for the pressure in the bulk,

$$\gamma_s = \rho_s\psi_s - \sum_{\alpha=0}^{N_s} \rho_{s,\alpha}\mu_{s,\alpha} \ . \tag{61}$$

Surface reaction rates. We use a linear relation between the reaction rate and the corresponding driving force,

$$R_s^i = -R_0^i \sum_{\alpha=0}^{N_S} \gamma_{s,\alpha}^i m_\alpha \mu_{s,\alpha}^e \ . \tag{62}$$

The kinetic coefficients $R_0^i > 0$ are called exchange rates.

We refer the reader to [4,17,18] where exponential non-linearities of Arrhenius-type were introduced in the constitutive equations for the surface reaction rates so that Butler-Volmer type equations come out instead of (62).

6.5 Introduction of stochastic objects in the constitutive model

The constitutive equations for the mass fluxes, reaction rates and stresses have been chosen so that the entropy production becomes a non-negative bilinear form which is zero in equilibrium. In this sense the constitutive equations are compatible with the 2nd law of thermodynamics.

The introduction of the quantities $f^\pm$ in the total mass fluxes (60c) is crucial in this work. For this reason we describe here the essential steps for the derivation of the constitutive relations (60b) and (60c).

Let us consider the entropy production ξ_s^ν due to the normal fluxes of momentum, heat and mass across the interface:

$$\begin{aligned}\xi_s^\nu =& \frac{1}{T_s}\Big[\!\Big[\Big(\sigma^{ij} - \Big(\rho\psi - \sum_{\alpha=0}^{N}\rho_\alpha\mu_\alpha\Big)\delta^{ij} - \Big(T_s\rho\big(\tfrac{\mu_0^e}{T} - \tfrac{\mu_{s,0}^e}{T_s}\big)\Big)\delta^{ij}\Big)(v^i - v_s^i)\nu_j\Big]\!\Big] \\ &+ \Big[\!\Big[\Big(q_\nu + \big(T\rho\eta + \sum_{\alpha=0}^{N}\rho_\alpha\mu_\alpha\big)(v_\nu - w_\nu)\Big)\Big(\frac{1}{T} - \frac{1}{T_s}\Big)\Big]\!\Big] \\ &- \Big[\!\Big[\sum_{\alpha=1}^{N} j_{\alpha,\nu}\Big(\tfrac{1}{T}(\mu_\alpha^e - \mu_0^e) - \tfrac{1}{T_s}(\mu_{s,\alpha}^e - \mu_{s,0}^e)\Big)\Big]\!\Big] \ . \end{aligned} \tag{63}$$

A derivation of the entropy production including tangential fluxes and surface reaction can be found in [3] and in the full case of coupled electro- and thermodynamics in [26]. Here q_ν denotes the normal heat flux and $\rho\eta$ is the entropy density of the corresponding bulk domains. The entropy density is related to the free energy by $\rho\eta = -\partial\rho\psi/\partial T$.

The entropy production can be extended by the following observation. The substitution

$$\mu_\alpha^e|_S^\pm \ \to \ \mu_\alpha^e|_S^\pm + \hat{f}^\pm \tag{64}$$

leaves the surface entropy production invariant. Here $\hat{f}^\pm$ are arbitrary functions of time and space defined at S that do not depend on the constituent index α.

Next we insert the constitutive equations (58) and (59) for the stress tensor and the pressure, respectively, in (63). Then we choose linear relations for the normal fluxes and obtain the relations

$$\rho(\boldsymbol{v}-\boldsymbol{w})\cdot\boldsymbol{\nu}|_S^{\pm} = \mp L_s^{\pm} T_s\big(\tfrac{\mu_0^e}{T}|_S^{\pm} - \tfrac{\mu_{s,0}^e}{T_s} + f^{\pm}\big)\ , \tag{65}$$

$$\Big(q_\nu + \big(T\rho\eta + \sum_{\alpha=0}^{N}\rho_\alpha\mu_\alpha\big)(v_\nu - w_\nu)\Big)|_S^{\pm} = \pm\Big(\kappa_s^{\pm} \mp \big(\rho(v_\nu-w_\nu)f\big)|_S^{\pm}\Big)\Big(\frac{1}{T|_S^{\pm}} - \frac{1}{T_s}\Big)\ , \tag{66}$$

$$\boldsymbol{j}_\alpha\cdot\boldsymbol{\nu}|_S^{\pm} = \mp M_{s,\alpha}^{\pm} T_s\big(\tfrac{1}{T}(\mu_\alpha^e - \mu_0^e)|_S^{\pm} - \frac{1}{T_s}(\mu_{s,\alpha}^e - \mu_{s,0}^e)\big)\ , \tag{67}$$

where we have replaced $\hat{f}$ by f which is defined as $f = (\frac{1}{T|_S^{\pm}} - \frac{1}{T_s})\hat{f}$. Here we are only interested in the isothermal case, thus we set $\kappa_s^{\pm} \to \infty$. Furthermore we assume that $\hat{f}$ is non-zero in the isothermal case. Thus we have a continuous temperature across the interface,

$$T_s = T|_S^{\pm}\ . \tag{68}$$

Then we obtain the constitutive equations (60b), (60c).

6.6 Special cases of the constitutive model

The constitutive equations for the mass fluxes can be written in the general form

$$F = KD\ , \tag{69}$$

where F represents a mass flux, $K > 0$ is the corresponding kinetic coefficient and D denotes the corresponding thermodynamic driving force.

In this section we consider two important regimes where the kinetic coefficients of the constitutive equations for the mass fluxes assume extreme values, viz.

- $K \to 0$ *slow regime* for diffusion and adsorption ,
- $K \to \infty$ *fast regime* for diffusion and adsorption.

In the slow regime $K \to 0$ the flux is zero and the driving force is independent of the flux. In the fast regime $K \to \infty$ the driving force is zero and the flux is determined by the balance equations. In particular the fast regime leads to some implications, which we study now in more details.

Infinite bulk mobilities. If the bulk mobility is very large, the fast regime $M_\alpha \to \infty$ is appropriate. For finite diffusion fluxes we must have

$$\nabla(\mu_\alpha^e - \mu_0^e) = 0 \ , \qquad \alpha = 1, 2, ..., N \ . \tag{70}$$

The equations (70) can be further simplified by the condition

$$\sum_{\alpha=0}^{N} m_\alpha n_\alpha \nabla \mu_\alpha^e = 0 \ . \tag{71}$$

This condition follows from a combination of (i) an identity between the spatial gradients of chemical potentials, (ii) the Gibbs-Duhem equation, and (iii) the local form of the quasi-static momentum balance [16].

Inserting (70) into (71) leads to

$$\nabla \mu_\alpha^e = 0 \ , \qquad \alpha = 0, 1, ..., N \ . \tag{72}$$

Thus the electrochemical potentials μ_α^e are the same in every point of the mixture.

Infinite surface mobilities. If the surface mobility is very large, the fast regime $M_{s,\alpha} \to \infty$ is appropriate. In an analogous manner as in the last paragraph we obtain constant surface electrochemical potentials,

$$\nabla_s \ \mu_{s,\alpha}^e = 0 \ , \qquad \alpha = 0, 1, ..., N_s \ . \tag{73}$$

We conclude that the surface electrochemical potentials $\mu_{s,\alpha}^e$ assume the same value in every point of a surface S.

Fast adsorption. The rate of an adsorption process, i.e. the transport of bulk matter to the surface, is determined by the kinetic coefficients $L_s^\pm$ and $M_{s,\alpha}^\pm$. We talk about fast adsorption of constituent A_0 if $L_s^\pm$ assumes a large value. In the fast regime $L_s^\pm \to \infty$, we have

$$\mu_0^e|_S^\pm - \mu_{s,0}^e + f^\pm = 0 \ . \tag{74}$$

Insertion into the constitutive equations (60b) of the other constituents then yields

$$\boldsymbol{j}_\alpha \cdot \boldsymbol{\nu}|_S^\pm = \mp M_{s,\alpha}^\pm (\mu_\alpha^e|_S^\pm - \mu_{s,\alpha}^e + f^\pm) \ . \tag{75}$$

If additionally the constituents A_α were also fast adsorbed so that the fast regime $M_{s,\alpha}^\pm \to \infty$ is appropriate, the adsorption relation (75) would implying

$$\mu_\alpha^e|_S^\pm - \mu_{s,\alpha}^e + f^\pm = 0 \ . \tag{76}$$

However the latter case is not considered here.

6.7 Application of the thermodynamic model to the LFP electrode

In this section we apply the thermodynamic model to the electrochemical cell presented in Figure 1. To this end several assumptions on both the balance equations and the kinetic coefficients are involved to simplify the general thermodynamic model of the last section. The final result will be the LFP electrode model introduced in Section 3.

Composition. The electrochemical cell consists of the many-particle cathode, an electrolyte and a metallic lithium anode as shown in Figure 1 and described in Section 2. For the modeling we decompose the total domain of the cell into volume domains and surface domains.

The $N_{\mathtt{P}}$ LFP particles occupy the volume domains Ω^i, $i = 1, 2, ..., N_{\mathtt{P}}$. The volume domains of the metallic substrate of the cathode, the electrolyte and the anode are denoted by $\Omega_{\mathtt{C}}$, $\Omega_{\mathtt{E}}$ and $\Omega_{\mathtt{A}}$, respectively.

The total domain is bounded by the upper and lower surfaces $S_{\mathtt{U}}$ and $S_{\mathtt{L}}$ and by the two electrode surfaces $S_{\mathtt{A}}$ and $S_{\mathtt{C}}$. A LFP particle $\mathtt{P}^i$ has a common interface with the electrolyte, $S^i_{\mathtt{E}}$, and may have an interface with another particle $\mathtt{P}^j$, which is indicated by S^{ij}. Moreover, the particle $\mathtt{P}^i$ may be in contact with the metallic substrate of the cathode via the interface $S^i_{\mathtt{C}}$. Thus the total interface of a particle $\mathtt{P}^i$ is given by $S^i = S^i_{\mathtt{C}} \cup S^i_{\mathtt{E}} \cup \sum_j S^{ij}$, where the sum runs over all particle-particle interfaces of particle $\mathtt{P}^i$. The interface between the metallic substrate of the cathode and the electrolyte, and the interface between the anode and the electrolyte are denoted by $S_{\mathtt{CE}}$ and $S_{\mathtt{AE}}$ respectively.

By convention the normal vector $\boldsymbol{\nu}$ of the surfaces $S^i_{\mathtt{E}}$, $S_{\mathtt{CE}}$, $S_{\mathtt{AE}}$ always points into the electrolyte. The normal vector of the surface $S^i_{\mathtt{C}}$ points into the metal substrate.

Each of the four bulk materials are mixtures with the following constituents: The metal substrate of the cathode and the lithium anode are binary mixtures of metal ions and electrons. We have $(\mathrm{Al}^+, \mathrm{e}^-)$ in the metal substrate of the cathode and $(\mathrm{Li}^+, \mathrm{e}^-)$ in the anode. A LFP particle is formed by the FePO_4 lattice and neutral lithium atoms Li. The constituents of the electrolyte are the lithium cations, Li^+, a solvent S and anions A^-. The constituent A_0 indicates (i) FePO_4 in the LFP particles, (ii) the metal ions Al^+ and Li^+ in cathode and anode, respectively, and (iii) the solvent in the electrolyte.

As assumed in the general setting the constituents of the bulk domains are likewise present on the various interfaces. Moreover, the carbon coating of the LFP particles is a part of the LFP surface. Therefore we have additional surface constituents, viz. (i) C^+ and free electrons e^- on the LFP surfaces.

On the LFP surfaces only one chemical reaction is considered,

$$\mathrm{Li}^+ + \mathrm{e}^- \rightleftharpoons \mathrm{Li} \quad \text{on } S^i \ . \tag{77}$$

Model equations for the LFP particles. The masses of lithium and iron phosphate within a particle $\mathtt{P}^i$ changes due to the normal component of the fluxes

$\boldsymbol{j}_{\mathrm{Li}}$ and $\boldsymbol{j}_{\mathrm{FePO_4}}$, respectively. The corresponding mass balances (36) read

$$\frac{d}{dt}\int_{\Omega^i}\rho_{\mathrm{Li}}\,dx = -\int_{S^i}\boldsymbol{j}_{\mathrm{Li}}\cdot\boldsymbol{\nu}\,da\ , \quad \frac{d}{dt}\int_{\Omega^i}\rho_{\mathrm{FePO_4}}\,dx = -\int_{S^i}\boldsymbol{j}_{\mathrm{FePO_4}}\cdot\boldsymbol{\nu}\,da\ . \tag{78}$$

The surface S^i of particle $\mathtt{P}^i$ consists of subsurfaces, viz. $S^i = S^i_{\mathtt{C}} \cup S^i_{\mathtt{E}} \cup \sum_j S^{ij}$.

To simplify the mass balances and to specify the lithium flux for the various subsurfaces of the particles we make the following assumptions:

A1 The phase transition within a single LFP particles is not observable on the time scale of charging/discharging.
A2 The diffusion of lithium within the LFP particles is fast, i.e. we assume that the fast diffusion regime applies in Ω^i.
A3 There is no lithium exchange between the metal cathode substrate and the particles, i.e. the slow regime for lithium adsorption applies at $S^i_{\mathtt{C}}$.
A4 The contact surface between to particles i and j is small compared to the total particle surface, thus the lithium exchange between to neighboring particles can be ignored. The slow regime for lithium adsorption applies on S^{ij}.
A5 The surface constituent $FePO_4$ is in equilibrium with the bulk constituent $FePO_4$ of the particles, i.e. we assume that the fast adsorption regime for $FePO_4$ adsorption applies on the LFP particle surface S^i.

Due to Assumptions A1 and A2 we can apply the reasoning leading to equation (72) of Section 6.6. The chemical potentials within the LFP particles (72) are constant in space, thus

$$\nabla\mu_{\mathrm{Li}} = 0 \qquad \text{and} \qquad \nabla\mu_{\mathrm{FePO_4}} = 0 \quad \text{in } \Omega^i\ . \tag{79}$$

The chemical potentials μ_{Li} and $\mu_{\mathrm{FePO_4}}$ only depend on the number densities of lithium and iron phosphate. We conclude

$$\nabla n_{\mathrm{Li}} = 0 \qquad \text{and} \qquad \nabla n_{\mathrm{FePO_4}} = 0 \quad \text{in } \Omega^i\ . \tag{80}$$

Thus Assumptions A1 and A2 imply that the particles are homogeneous. Note that the value of the number densities depends on the particle index, i.e the number densities assume different values in the particles.

Moreover Assumptions A3 and A4 imply that the normal component of the lithium fluxes are zero at $S^i_{\mathtt{C}}$ and S^{ij}. Thus we have

$$m_{\mathrm{Li}}\frac{d}{dt}(V^i n^i_{\mathrm{Li}}) = -\int_{S^i_{\mathtt{E}}}\boldsymbol{j}_{\mathrm{Li}}\cdot\boldsymbol{\nu}da \qquad \text{and} \qquad m_{\mathrm{FePO_4}}\frac{d}{dt}(V^i n^i_{\mathrm{FePO_4}}) = -\int_{S^i_{\mathtt{E}}}\boldsymbol{j}_{\mathrm{FePO_4}}\cdot\boldsymbol{\nu}da\ . \tag{81}$$

Due to Assumption A4 for $FePO_4$ we obtain the adsorption relation

$$\mu_{\mathrm{FePO_4}} - \mu_{s,\mathrm{FePO_4}} + f^- = 0 \qquad \text{on } S^i_{\mathtt{E}}. \tag{82}$$

Then the lithium flux on $S^i_{\mathtt{E}}$ is given by

$$\boldsymbol{j}_{\mathrm{Li}} \cdot \boldsymbol{\nu}|^-_{S^i_E} = \tfrac{m_{\mathrm{Li}}}{k_B T} k_{\mathrm{Li}}(\mu_{\mathrm{Li}} - \mu_{s,\mathrm{Li}} + f^-) \qquad \text{on } S^i_{\mathtt{E}} \quad \text{with} \quad k_{\mathrm{Li}} = M^-_{s,\mathrm{Li}} \tfrac{k_B T}{m_{\mathrm{Li}}}. \tag{83}$$

Two remarks: i) Li and $FePO_4$ have no electric charge, thus in equations (82) and (83) the electrochemical potentials are equal to the chemical potentials. ii) Up to now only the bulk chemical potentials μ_α are constant in space, the surface quantities $\mu_{s,\alpha}$ and f^- may still variate on the particle surface.

Model equations for surfaces of the LFP particles. Next we apply the surface mass balance (38) for lithium to the surface S^i of particle $\mathtt{P}^i$.

For its exploitation we introduce further assumptions:

A6 The tangential transport of the surface constituents $\mathrm{Li}, \mathrm{Li}^+, \mathrm{e}^-, S, A^-$ is fast, i.e. we apply the fast regime for surface diffusion.
A7 The surface constituents C^+ and $FePO_4$ move with the particle surfaces, i.e. the tangential fluxes $\boldsymbol{j}_{s,\mathrm{C}}$, $\boldsymbol{j}_{s,\mathrm{FePO_4}}$ are zero.
A8 On S^i the changes in the masses of all surface constituents are determined by stationary processes.
A9 The chemical reaction $\mathrm{Li}^+ + \mathrm{e}^- \rightleftharpoons \mathrm{Li}$ exclusively occurs on the subsurface $S^i_{\mathtt{E}}$.

A common exploitation of Assumptions A6 and A7 and the reasoning from Section 6.6 imply that the surface electrochemical potentials $\mu^e_{s,\alpha}$ do not depend on the position of the surface S^i,

$$\nabla_s \mu^e_{s,\alpha} = 0, \qquad \text{for } \alpha = \mathrm{Li}, \mathrm{Li}^+, \mathrm{e}^-, \mathrm{C}^+, S, A^-, \mathrm{FePO_4} \quad \text{on } S^i_{\mathtt{C}}, S^i_{\mathtt{E}}, S^{ij}\ . \tag{84}$$

The Assumptions A8 and A9 simplify the surface mass balances for surface constituents. For $\alpha = \mathrm{Li}, \mathrm{Li}^+, \mathrm{e}^-, S, A^-$ we obtain

$$\int_{\partial S} \boldsymbol{j}_{s,\alpha} \cdot \boldsymbol{e}\, dl = -\int_S [\![\boldsymbol{j}_\alpha \cdot \boldsymbol{\nu}]\!]\, da + m_\alpha \gamma_{s,\alpha} \int_S R_s\, da \qquad \text{for} \quad S = S^i_{\mathtt{C}}, S^i_{\mathtt{E}}, S^{ij}\ . \tag{85}$$

These equations are used to determine the corresponding tangential fluxes $\boldsymbol{j}_{s,\alpha}$. The Assumptions A7 and A8 yield that the surface mass balance for C^+ is identically satisfied, and we have for $FePO_4$

$$\int_S \boldsymbol{j}_{\mathrm{FePO_4}} \cdot \boldsymbol{\nu}\, da = 0 \qquad \text{for} \quad S = S^i_{\mathtt{C}}, S^i_{\mathtt{E}}, S^{ij}\ . \tag{86}$$

Finally due to equation (62) and Assumption A7 the surface reaction rate reads

$$R_s = R^{\mathtt{E}}_0(m_{\mathrm{Li}^+}\mu^e_{s,\mathrm{Li}^+} + m_{\mathrm{e}^-}\mu^e_{s,\mathrm{e}^-} - m_{\mathrm{Li}}\mu^e_{s,\mathrm{Li}}) \quad \text{on} \quad S^i_{\mathtt{E}}\ . \tag{87}$$

Model equations for the electrolyte. The boundary of the electrolyte domain $\Omega_{\mathtt{E}}$ is given by $S_{\mathtt{E}} = \sum_i S_{\mathtt{E}}^i \cup S_{\mathtt{CE}} \cup S_{\mathtt{AE}} \cup S_{\mathtt{U}} \cup S_{\mathtt{L}}$.

We characterize the electrolyte by the following assumptions:

A10 The diffusion of the electrolytic constituents is fast.

A11 The masses of the electrolytic constituents are determined by a stationary process.

A12 There is no adsorption on the surface $S_{\mathtt{CE}}$ of the metallic substrate and on the upper and lower surfaces $S_{\mathtt{U}}$ and $S_{\mathtt{L}}$, respectively. Thus we assume for the electrolytic constituents the slow adsorption regime at $S_{\mathtt{CE}}, S_{\mathtt{U}}, S_{\mathtt{L}}$.

A13 On both the particle-electrolyte surface $S_{\mathtt{E}}^i$ and the anode substrate surface $S_{\mathtt{AE}}$ we have fast adsorption of the solvent and the anions.

A14 The quantity f^+ is set to zero at the anode surface, i.e. we ignore stochastic effects on the anode surface.

According to Section 6.6 the fast diffusion regime, Assumption A10, implies constant electrochemical potentials of the electrolyte species,

$$\nabla \mu_\alpha^e = 0 \qquad \text{for } \alpha = \mathrm{Li}^+, A, S \quad \text{in } \Omega_{\mathtt{E}} \,. \tag{88}$$

In contrast to the LFP particles there are charged constituents in the electrolyte. Thus we cannot replace the electrochemical potentials by the chemical potential. Moreover we cannot conclude that the corresponding number densities are constant.

Assumptions A11 and A12 simplify the bulk mass balance in the electrolyte to

$$0 = \sum_{i=1}^{N_{\mathtt{P}}} \int_{S_{\mathtt{E}}^i} \boldsymbol{j}_\alpha \cdot \boldsymbol{\nu} \, da + \int_{S_{\mathtt{AE}}} \boldsymbol{j}_\alpha \cdot \boldsymbol{\nu} \, da \qquad \alpha = \mathrm{Li}^+, A, S \,. \tag{89}$$

Finally due to Assumption A13 the anions and the solvent must satisfy

$$\mu_\alpha^e - \mu_{s,\alpha}^e + f^+ = 0 \qquad \text{for } \alpha = A, S \qquad \text{on } S_{\mathtt{E}}^i \,, S_{\mathtt{AE}} \,. \tag{90}$$

Then the adsorption fluxes of lithium are represented by

$$\boldsymbol{j}_{\mathrm{Li}^+} \cdot \boldsymbol{\nu}|_{S_E^i}^+ = -M_{s,\mathrm{Li}^+}^{\mathtt{E}} (\mu_{\mathrm{Li}^+}^e - \mu_{s,\mathrm{Li}^+}^e + f^+) \qquad \text{on } S_{\mathtt{E}}^i \,, \tag{91}$$

$$\boldsymbol{j}_{\mathrm{Li}^+} \cdot \boldsymbol{\nu}|_{S_{\mathtt{AE}}}^+ = -M_{s,\mathrm{Li}^+}^{\mathtt{AE}} (\mu_{\mathrm{Li}^+}^e - \mu_{s,\mathrm{Li}^+}^e) \qquad \text{on } S_{\mathtt{AE}} \,. \tag{92}$$

Note that we may have different kinetic coefficients M_{s,Li^+} on $S_{\mathtt{E}}^i$ and $S_{\mathtt{AE}}$. This is indicated by the superscripts. The representation (92) relies on Assumption A14.

Model equations for the electrolyte-anode interface. Both the electrolyte and the metal lithium anode contain lithium ions with the same electric charge number. Nevertheless lithium ions in the liquid electrolyte and the solid lithium anode are treated as different constituents in this model because lattice ions have different electrochemical properties as solute ions. At the interface $S_{\mathtt{AE}}$ the different lithium ions are indicated by the subscripts $\mathtt{E}$ and $\mathtt{A}$. The electrolytic

lithium ions $\mathrm{Li}^+_{\mathtt{E}}$ can freely move on $S_{\mathtt{AE}}$ whereas the metallic lithium ions of the anode $\mathrm{Li}^+_{\mathtt{A}}$ are fixed in the crystal lattice of the lithium metal. In this context on the anode surface $S_{\mathtt{AE}}$ we have the surface reaction

$$\mathrm{Li}^+_{\mathtt{E}} \rightleftharpoons \mathrm{Li}^+_{\mathtt{A}} \qquad \text{on } S_{\mathtt{AE}} \,. \tag{93}$$

The surface $S_{\mathtt{AE}}$ is characterized by the assumptions

A15 The tangential surface transport of all surface constituents is fast, i.e. the fast regime for surface diffusion is assumed.

A16 On $S_{\mathtt{AE}}$ the masses of all surface constituents are determined by a stationary processes, and there is no tangential mass flux over the boundary $\partial S_{\mathtt{AE}}$.

Assumption A15 implies that the surface electrochemical potentials do not depend on the surface point,

$$\nabla_s \mu^e_{s,\alpha} = 0 \qquad \text{for } \alpha = \mathrm{Li}^+_{\mathtt{A}}, \mathrm{Li}^+_{\mathtt{E}}, \mathrm{e}^-, A, S \quad \text{on } S_{\mathtt{AE}}. \tag{94}$$

Assumption A16 yields for the electrolytic constituents

$$0 = -\int_{S_{\mathtt{AE}}} \boldsymbol{j}_{\mathrm{Li}^+_{\mathtt{E}}} \cdot \boldsymbol{\nu}\, da - m_{\mathrm{Li}^+} \int_{S_{\mathtt{AE}}} R_{s,\mathtt{AE}}\, da \qquad \text{and} \quad 0 = \int_{S_{\mathtt{AE}}} \boldsymbol{j}_\alpha \cdot \boldsymbol{\nu}\, da \qquad \alpha = A, S \,, \tag{95}$$

and for the anode constituents

$$0 = \int_{S_{\mathtt{AE}}} \boldsymbol{j}_{\mathrm{Li}^+_{\mathtt{A}}} \cdot \boldsymbol{\nu}\, da + m_{\mathrm{Li}^+} \int_{S_{\mathtt{AE}}} R_{s,\mathtt{AE}}\, da \qquad \text{and} \qquad 0 = \int_{S_{\mathtt{AE}}} \boldsymbol{j}_{\mathrm{e}^-} \cdot \boldsymbol{\nu}\, da \,. \tag{96}$$

According to (62) the reaction rate $R_{s,\mathtt{AE}}$ reads

$$R_{s,\mathtt{AE}} = R_0^{\mathtt{AE}} m_{\mathrm{Li}^+} (\mu^e_{s,\mathrm{Li}^+_{\mathtt{E}}} - \mu^e_{s,\mathrm{Li}^+_{\mathtt{A}}}) \qquad \text{on } S_{\mathtt{AE}} \,. \tag{97}$$

Model equations for the metal substrate-electrolyte interface. Here we assume

A17 The tangential transport of all surface constituents on $S_{\mathtt{CE}}$ is fast, i.e. we apply the fast regime for surface diffusion.

This Assumption implies that on $S_{\mathtt{CE}}$ the electrochemical potentials are constant in space,

$$\nabla_s \mu^e_{s,\alpha} = 0 \qquad \text{for } \alpha = \mathrm{Al}^+, \mathrm{e}^-, \mathrm{Li}^+, A, S \quad \text{on } S_{\mathtt{CE}} \,. \tag{98}$$

Model equations for the metals. Both the anode and the substrate of the cathode are metals. We assume

A18 The diffusion of the electrons is fast.
A19 There is global charge neutrality in both metals.
A20 On metal surfaces we have fast adsorption of both electrons and metal ions.

Assumption A18 implies in the bulk domains

$$\nabla \mu^e_\alpha = 0 \qquad \alpha = \mathrm{e}^-, \mathrm{Li}^+, \mathrm{Al}^+ \quad \text{in} \quad \Omega_{\mathtt{A}}, \Omega_{\mathtt{C}} \ . \tag{99}$$

We conclude from Assumption A19 that the volume integral under the time derivative of the charge balance (50) vanishes. Thus the charge balance for the anode reads

$$0 = \int_{S_{\mathtt{A}}} \boldsymbol{j}^e \cdot \boldsymbol{\nu} \, da + \int_{S_{\mathtt{AE}}} \boldsymbol{j}^e \cdot \boldsymbol{\nu} \, da \ . \tag{100}$$

The charge balance for the metal substrate of the cathode is represented in a similar manner.

Assumption A20 is now applied to the constitutive equations (60b) and (60c) for adsorption. For the anode it follows

$$\mu^e_\alpha = \mu^e_{s,\alpha} \qquad \alpha = \mathrm{e}^-, \mathrm{Li}^+ \qquad \text{on } S_{\mathtt{AE}}, S_{\mathtt{A}} \ , \tag{101}$$

and for the metal substrate of the cathode we obtain

$$\mu^e_\alpha = \mu^e_{s,\alpha} \qquad \alpha = \mathrm{e}^-, \mathrm{Al}^+ \qquad \text{on } S^i_{\mathtt{C}}, S_{\mathtt{C}}, S_{\mathtt{CE}} \ . \tag{102}$$

Properties of electrochemical potentials at the contact lines. So far our thermodynamic model exclusively treated bulk and surface domains. Additionally we meet contact lines between the different subsurfaces. However, here we will not enter a careful thermodynamic treatment of line phenomena, rather we simply proceed with the Assumption

A21 The electrochemical potentials of electrons, lithium ions and lithium atoms of the two intersecting surfaces are continuous at the corresponding contact line.

This assumption can be derived within thermodynamics of lines if one assumes that the contact line is itself not a carrier of mass, momentum and energy.

The Assumption A21 has far-reaching consequences here: The surface electrochemical potentials of electrons, lithium ions and lithium atoms, respectively, assume the same values on the LFP particle surfaces, i.e. they do not depend on the particle index,

$$\mu^e_{s,\alpha}|_{S^i} = \mu^e_{s,\alpha} \qquad \text{for } \alpha = \mathrm{e}^-, \mathrm{Li}^+, \mathrm{Li} \quad \text{on } S^i \ . \tag{103}$$

Remarks on the momentum balance equation. At first glance the reader may think that until now the momentum balance has not been used. However, this is not the case. In particular, the exploitation of the fast diffusion regime heavily relies on the momentum balance. For example, the momentum balance is needed to conclude that $\nabla(\mu_\alpha^e - \mu_0^e) = 0$ for $\alpha = 1, 2, ..., N$ implies $\nabla\mu_\alpha^e = 0$ for $\alpha = 0, 1, 2, ..., N$, see [16,17] for more details.

Constitutive theory. Until now explicit constitutive equations for the chemical potentials and the pressure were not needed. Moreover an inspection of the model equations reveals that in this study explicit constitutive equations are exclusively needed for the LFP particles. These will be given now. Recall both chemical potentials and pressure are derived from a single free energy function. In [13,14] a free energy function for LFP is introduced, incorporating (i) the mixing entropy of the distribution of lithium over the interstitial lattices sites of the iron phosphate lattice and (ii) the mechanical deformation of LFP due to the intercalation process. The resulting representations of chemical potentials and the pressure are

$$\mu_{\mathrm{Li}} = \mu_{\mathrm{Li}}^{\mathrm{ref}}(T,p) + \tfrac{1}{m_{\mathrm{Li}}}\Big(L(1-2y) + k_B T\big(\ln(y) - \ln(1-y)\big)\Big)\,, \tag{104}$$

$$\mu_{\mathrm{FePO_4}} = \mu_{\mathrm{FePO_4}}^{\mathrm{ref}}(T,p) + \tfrac{1}{m_{\mathrm{FePO_4}}}\Big(Ly^2 + k_B T\ln(1-y)\Big)\,, \tag{105}$$

$$p = p^{\mathrm{ref}} + K\big((v_{\mathrm{FePO_4}}^{\mathrm{ref}} n_{\mathrm{FePO_4}} + v_{\mathrm{Li}}^{\mathrm{ref}} n_{\mathrm{Li}}) - 1\big)\,, \tag{106}$$

where we have introduced the lithium mole fraction $y = n_{\mathrm{Li}}/n_{\mathrm{FePO_4}}$. The reference chemical potentials $\mu_\alpha^{\mathrm{ref}}$ are in general function of temperature and pressure. Here the $\mu_\alpha^{\mathrm{ref}}$ are calculated by $\mu_{\mathrm{Li}}^{\mathrm{ref}}(T,p) = g_{\mathrm{Li}}(T) + v_{\mathrm{Li}}(p^{\mathrm{ref}} + K\ln(\frac{p-p^{\mathrm{ref}}}{K} + 1))$ and $\mu_{\mathrm{FePO_4}}^{\mathrm{ref}}(T,p) = g_{\mathrm{FePO_4}}(T) + v_{\mathrm{FePO_4}}(p^{\mathrm{ref}} + K\ln(\frac{p-p^{\mathrm{ref}}}{K} + 1))$. Thus the temperature dependence is left unspecified and the pressure contribution describes linear elastic behavior with volume expansion due to intercalation. The positive constants $v_{\mathrm{FePO_4}}^{\mathrm{ref}}$ and $v_{\mathrm{Li}}^{\mathrm{ref}}$ are the specific volumes of iron phosphate and lithium in LFP. Here p^{ref} is a reference pressure and K is the bulk modulus of LFP. In general the bulk modulus is a function of the lithium content in LFP. For simplicity this is ignored here and K is assumed to be constant.

Volume expansion and surface momentum balance. The intercalation of lithium into the iron phosphate lattice is accompanied by a volume expansion. This is incorporated into the model by the constitutive relation (106). In this study, however, we want to keep the model as simple as possible and neglect the volume expansion. We thus assume

A22 The volume expansion due to intercalation of lithium is negligible, i.e. we set $v_{\mathrm{Li}}^{\mathrm{ref}} = 0$.

It is important to note that the pressure in each particle is still different due to surface tension and mean curvature of the particles. To avoid this complexity a further model simplification becomes necessary. It concerns the surface balance of momentum (45). We assume

A23 The normal component of the total stress $\boldsymbol{\Sigma}$ is continuous at the particle surfaces S^i, i.e.

$$[\![\boldsymbol{\nu}\cdot\boldsymbol{\Sigma}\cdot\boldsymbol{\nu}]\!]=0 \qquad \text{at } S^i\ . \tag{107}$$

This assumption is satisfied if the product of mean curvature and surface stress is small compared to the total stress.

The outer pressure p_0 acting on the cell surface, i.e. the pressure on $S_{\mathtt{C}}\cup S_{\mathtt{A}}\cup S_{\mathtt{U}}\cup S_{\mathtt{L}}$, is constant. Under the Assumptions A22 and A23 the momentum balance equation yields that the pressure within each particles is given by the outer pressure,

$$p=p_0\ . \tag{108}$$

This implies that the particle density $n_{\mathrm{FePO_4}}$ of the iron phosphate lattice of the particles is determined by the constant specific volume,

$$n_{\mathrm{FePO_4}}=(v^{\mathrm{ref}}_{\mathrm{FePO_4}})^{-1} \qquad \text{for all } \ \Omega^i\ . \tag{109}$$

Moreover we conclude from the mass balance equations (81) and (86) of $\mathrm{FePO_4}$ that the volumes of the LFP particles are time independent,

$$\tfrac{d}{dt}V^i=0 \qquad \text{for all } \ i=1,\dots,N_{\mathtt{P}}\ . \tag{110}$$

Constant number density of iron phosphate and constant pressure within the particles imply that the chemical potentials of lithium only change if the lithium mole fraction $y=n_{\mathrm{Li}}/n_{\mathrm{FePO_4}}$ changes,

$$\mu_{\mathrm{Li}}=\mu_{\mathrm{Li}}(y)\ . \tag{111}$$

6.8 Evolution equations for the lithium mole fractions of the LFP electrode model

The balance equation (81) and the corresponding constitutive equation for the mass flux (83) form the basis of the LFP electrode model.

Due to the assumptions of the last subsection, the lithium mass flux normal to the surface $S^i_{\mathtt{E}}$ is spatially constant if we assume a spatially constant f^- on $S^i_{\mathtt{E}}$,

$$\boldsymbol{j}_{\mathrm{Li}}\cdot\boldsymbol{\nu}|^-_{S^i_{\mathtt{E}}}=\tfrac{m_{\mathrm{Li}}}{k_BT}k_{\mathrm{Li}}\Big(\mu_{\mathrm{Li}}(y^i)-\mu_{s,\mathrm{Li}}+f^{i,-}\Big) \qquad \text{at } S^i_{\mathtt{E}}\ . \tag{112}$$

Finally we use (109),(110) and (112) so that the lithium mass balance equations (83) becomes the central evolution equation of this study: For $i=1,\dots,N_{\mathtt{P}}$

$$\frac{dy^i}{dt}=\frac{1}{\tau^i}\frac{m_{\mathrm{Li}}}{k_BT}\big(\mu_{s,\mathrm{Li}}-\mu_{\mathrm{Li}}(y^i)-f^{i,-}\big) \quad \text{with} \quad \frac{1}{\tau^i}=\frac{k_{\mathrm{Li}}}{m_{\mathrm{Li}}n_{\mathrm{FePO_4}}}\frac{A^i_{\mathtt{E}}}{V^i}\ . \tag{113}$$

Taking

$$f^{i,-}=\frac{Tk_B}{m_{\mathrm{Li}}}\big(\sqrt{\frac{2}{\tau^i}}\nu^i\dot{W}^i-\dot{Z}\big) \tag{114}$$

we find the SDE system (12) that we were looking for.

6.9 Wiener process

In this section we clarify the meaning of the term $\dot{W}^i$ that appears in the expression (114) for the average of $f^{i,-}$. This is formally the white noise, that is the time derivative of a Brownian motion W (introduced in Section 3.2). Now such a derivative is not well-defined: as well-known, the typical paths of the Brownian motion are continuous but not differentiable. However equation (12) makes still sense: from a mathematical perspective, (12) does require only the definition of W, not of its derivative, moreover the SDE theory allows to control the so-called Itô integrals ($\int_0^t X dW$ for certain stochastic processes X) even if dW is not defined.

From a physical perspective, one should think of $f^{-,i}$ not as the (scaled) white noise but as a suitable approximation of it (that is, one should replace $\dot{W}^i$ by the time derivative of a smooth approximation of the Bronwian motion W^i). Possible drawbacks may come from guaranteeing compatibility with other assumptions: for example, equation (82), for $f^{-,i}$ approximation of white noise, implies that $\mu_{s,\mathrm{FePO_4}}$ should also be a highly oscillating functions assuming large values. We do not discuss these issues here.

6.10 Charge transport

The charge is transported by the lithium ions from the anode to the cathode, whereby the electrons have to flow through an electric device. The electric device is connected to the battery via the surfaces $S_{\mathtt{A}}$ and $S_{\mathtt{C}}$.

We define the electric current I of the battery by the electric current density $\boldsymbol{j}^e$ which flows through the outer anode surface $S_{\mathtt{A}}$., viz.

$$I = \int_{S_{\mathtt{A}}} \boldsymbol{j}^{\mathrm{e}} \cdot \boldsymbol{\nu}\, da \qquad \text{with} \quad \boldsymbol{j}^{\mathrm{e}} = \sum_{\alpha=\mathrm{e}^-,\mathrm{Li}^+} \frac{e_0 z_\alpha}{m_\alpha} \boldsymbol{j}_\alpha \ . \tag{115}$$

Using the mass balances (100), (95), (96), (89) and (85) we conclude

$$I = \frac{e_0}{m_{\mathrm{Li}^+}} \int_{S_{\mathtt{AE}}} \boldsymbol{j}_{\mathrm{Li}^+} \cdot \boldsymbol{\nu}\, da = -\frac{e_0}{m_{\mathrm{Li}^+}} \sum_{i=1}^{N_{\mathtt{P}}} \int_{S_{\mathtt{E}}^i} \boldsymbol{j}_{\mathrm{Li}^+} \cdot \boldsymbol{\nu}\, da = -\frac{e_0}{m_{\mathrm{Li}}} \sum_{i=1}^{N_{\mathtt{P}}} \int_{S_{\mathtt{E}}^i} \boldsymbol{j}_{\mathrm{Li}} \cdot \boldsymbol{\nu}\, da \ . \tag{116}$$

In a further step we replace the lithium fluxes of the electrolyte side by the fluxes of stored lithium in the LFP particles. To this end we use equation (81) and then obtain a relation between the current and the total lithium mole fraction that we seek for,

$$I \quad = e_0 n_{\mathrm{FePO_4}} V_{\mathtt{P}} \frac{d}{dt}\Big(\sum_{i=1}^{N_{\mathtt{P}}} \frac{V^i}{V_{\mathtt{P}}} y^i \Big) \quad = e_0 n_{\mathrm{FePO_4}} V_{\mathtt{P}} \frac{dq}{dt} \ . \tag{117}$$

This equation expresses the intuitive relation that the electric current is directly related to the amount of stored lithium in the ensemble of LFP particles.

A further important observation is that the relation (117) is exclusively derived from balance equations. Thus the equation (117) is independent of the constitutive equations and especially of the materials at hand. Note, we have assumed that the mass balances at the surfaces, in both metals and electrolyte are stationary. This implies that the electric charge is exclusively stored in the LFP particles. In particular without the stationary balance equations for the LFP particles, a surface contribution would appear in (117).

6.11 Battery voltage

The electric potential difference between the metallic substrate of the cathode at the surface $S_{\mathtt{C}}$ and of the anode at $S_{\mathtt{A}}$ defines the cell voltage

$$U = \varphi|_{S_{\mathtt{C}}} - \varphi|_{S_{\mathtt{A}}} \ . \tag{118}$$

Herein we use the electrochemical potentials, $\mu^e_\alpha = \mu_\alpha + \frac{e_0 z_\alpha}{m_\alpha}\,\varphi$, for the electrons in the substrate of the cathode and for lithium ions in the anode to obtain

$$U = \frac{m_{\mathrm{e}^-}}{e_0}(\mu_{\mathrm{e}^-} - \mu^e_{\mathrm{e}^-})|_{S_{\mathtt{C}}} + \frac{m_{\mathrm{Li}^+}}{e_0}(\mu_{\mathrm{Li}^+_{\mathtt{A}}} - \mu^e_{\mathrm{Li}^+_{\mathtt{A}}})|_{S_{\mathtt{A}}} \ . \tag{119}$$

The assumptions of fast diffusion and fast adsorption for the electrons in the cathode imply that its electrochemical potential $\mu^e_{e^-}$ is the same everywhere in the cathode where electrons exist. In particular we have $\mu^e_{s,\mathrm{e}^-}|_{S_{\mathtt{E}}} = \mu^e_{\mathrm{e}^-}|_{S_{\mathtt{C}}}$, where $S_{\mathtt{E}}$ is an abbreviation for $S_{\mathtt{E}} = \cup_i S^i_{\mathtt{E}}$. The fast diffusion assumption for the anode implies that the electrochemical potential of the lithium ions in the anode is everywhere the same and thus we have $\mu^e_{s,\mathrm{Li}^+_{\mathtt{A}}}|_{S_{\mathtt{AE}}} = \mu^e_{\mathrm{Li}^+_{\mathtt{A}}}|_{S_{\mathtt{A}}}$.

Thus we may write

$$U = \frac{m_{\mathrm{e}^-}}{e_0}\big(\mu_{\mathrm{e}^-}|_{S_{\mathtt{C}}} - \mu^e_{s,\mathrm{e}^-}|_{S_{\mathtt{E}}}\big) + \frac{m_{\mathrm{Li}^+}}{e_0}\big(\mu_{\mathrm{Li}^+_{\mathtt{A}}}|_{S_{\mathtt{A}}} - \mu^e_{s,\mathrm{Li}^+_{\mathtt{A}}}|_{S_{\mathtt{AE}}}\big) \ . \tag{120}$$

In order to generate differences that can be represented by adsorption fluxes and the reaction rate, respectively, we add some new terms that cancel each other,

$$\begin{aligned}
U =& \tfrac{1}{e_0}\big(m_{\mathrm{Li}^+}\mu_{\mathrm{Li}^+_{\mathtt{A}}}|_{S_{\mathtt{A}}} + m_{\mathrm{e}^-}\mu_{\mathrm{e}^-}|_{S_{\mathtt{C}}}\big) \\
&- \tfrac{1}{e_0}\big(m_{\mathrm{Li}^+}\mu^e_{s,\mathrm{Li}^+_{\mathtt{A}}}|_{S_{\mathtt{AE}}} - m_{\mathrm{Li}^+}\mu^e_{s,\mathrm{Li}^+}|_{S_{\mathtt{AE}}}\big) \\
&- \tfrac{1}{e_0}\big(m_{\mathrm{Li}^+}\mu^e_{s,\mathrm{Li}^+}|_{S_{\mathtt{AE}}} - m_{\mathrm{Li}^+}\mu^e_{\mathrm{Li}^+}|^+_{S_{\mathtt{AE}}}\big) \\
&- \tfrac{1}{e_0}\big(m_{\mathrm{Li}^+}\mu^e_{\mathrm{Li}^+}|^+_{S_{\mathtt{AE}}} - m_{\mathrm{Li}^+}\mu^e_{\mathrm{Li}^+}|^+_{S_{\mathtt{E}}}\big) \\
&- \tfrac{1}{e_0}\big(m_{\mathrm{Li}^+}\mu^e_{\mathrm{Li}^+}|^+_{S_{\mathtt{E}}} - m_{\mathrm{Li}^+}\mu^e_{s,\mathrm{Li}^+}|_{S_{\mathtt{E}}}\big) \\
&- \tfrac{1}{e_0}\big(m_{\mathrm{Li}^+}\mu^e_{s,\mathrm{Li}^+}|_{S_{\mathtt{E}}} + m_{\mathrm{e}^-}\mu^e_{s,\mathrm{e}^-}|_{S_{\mathtt{E}}} - m_{\mathrm{Li}}\mu^e_{s,\mathrm{Li}}|_{S_{\mathtt{E}}}\big) \\
&- \tfrac{m_{\mathrm{Li}}}{e_0}\sum_{i=1}^{N_{\mathtt{P}}}\frac{A^i_{\mathtt{E}}}{A_{\mathtt{E}}}(\mu^e_{s,\mathrm{Li}} - \mu^e_{\mathrm{Li}})|_{S^i_{\mathtt{E}}} - \tfrac{m_{\mathrm{Li}}}{e_0}\sum_{i=1}^{N_{\mathtt{P}}}\frac{A^i_{\mathtt{E}}}{A_{\mathtt{E}}}\mu^e_{\mathrm{Li}}|_{S^i_{\mathtt{E}}} \ .
\end{aligned} \tag{121}$$

Next we use the relations (97),(92),(88),(91),(87), (83) and (111) to replace in (121) the chemical potential differences,

$$\begin{aligned} U =& \tfrac{1}{e_0}\big(m_{\mathrm{Li^+}}\mu_{\mathrm{Li}^+_{\mathtt{A}}}|_{S_{\mathtt{A}}} + m_{\mathrm{e^-}}\mu_{\mathrm{e^-}}|_{S_{\mathtt{C}}}\big) \\ & \tfrac{1}{e_0 R_0^{\mathtt{AE}}} R_{s,\mathtt{AE}} \\ & - \tfrac{m_{\mathrm{Li^+}}}{e_0 M^{\mathtt{AE}}_{s,\mathrm{Li^+}}} \tfrac{1}{A_{\mathtt{AE}}} \int_{S_{\mathtt{AE}}} \boldsymbol{j}_{\mathrm{Li^+}} \cdot \boldsymbol{\nu}\, da \\ & + \tfrac{m_{\mathrm{Li^+}}}{e_0 M^{\mathtt{E}}_{s,\mathrm{Li^+}}} \sum_{i=1}^{N_{\mathtt{P}}} \tfrac{A^i_{\mathtt{E}}}{A_{\mathtt{E}}} (\boldsymbol{j}_{\mathrm{Li^+}} \cdot \boldsymbol{\nu})|_{S^i_{\mathtt{E}}} + \tfrac{m_{\mathrm{Li}}}{e_0} \sum_{i=1}^{N_{\mathtt{P}}} \tfrac{A^i_{\mathtt{E}}}{A_{\mathtt{E}}} f^+|_{S^i_{\mathtt{E}}} \\ & - \tfrac{1}{e_0 R_0^{\mathtt{E}}} R_s \\ & + \tfrac{k_B T}{e_0} \tfrac{1}{k_{\mathrm{Li}}} \sum_{i=1}^{N_{\mathtt{P}}} \tfrac{A^i_{\mathtt{E}}}{A_{\mathtt{E}}} \boldsymbol{j}_{\mathrm{Li}} \cdot \boldsymbol{\nu}|_{S^i_{\mathtt{E}}} - \tfrac{m_{\mathrm{Li}}}{e_0} \sum_{i=1}^{N_{\mathtt{P}}} \tfrac{A^i_{\mathtt{E}}}{A_{\mathtt{E}}} f^-|_{S^i_{\mathtt{E}}} - \tfrac{m_{\mathrm{Li}}}{e_0} \sum_{i=1}^{N_{\mathtt{P}}} \tfrac{A^i_{\mathtt{E}}}{A_{\mathtt{E}}} \mu_{\mathrm{Li}}(y^i)\ . \end{aligned} \tag{122}$$

Note that a choice of the function f^+ has not been made up to now. Therefore we can use $f^+ = f^-$ to eliminate f^- in (122). In the next step we replace the mass fluxes and the reaction rate by the current I. To this end we use the equations (95), (116) and (85) and obtain

$$\begin{aligned} U =& \tfrac{1}{e_0}\big(m_{\mathrm{Li^+}}\mu_{\mathrm{Li}^+_{\mathtt{A}}}|_{S_{\mathtt{A}}} + m_{\mathrm{e^-}}\mu_{\mathrm{e^-}}|_{S_{\mathtt{C}}}\big) \\ & - \Big(\tfrac{1}{e_0^2 R_0^{\mathtt{AE}}} \tfrac{1}{A_{\mathtt{AE}}} + \tfrac{(m_{\mathrm{Li^+}})^2}{e_0^2 M^{\mathtt{AE}}_{s,\mathrm{Li^+}}} \tfrac{1}{A_{\mathtt{AE}}} + \tfrac{(m_{\mathrm{Li^+}})^2}{e_0^2 M^{\mathtt{E}}_{s,\mathrm{Li^+}}} \tfrac{1}{A_{\mathtt{E}}} + \tfrac{1}{e_0^2 R_0^{\mathtt{E}}} \tfrac{1}{A_{\mathtt{E}}} + \tfrac{m_{\mathrm{Li}} k_B T}{e_0^2} \tfrac{1}{k_{\mathrm{Li}}} \tfrac{1}{A_{\mathtt{E}}}\Big) I \\ & - \tfrac{m_{\mathrm{Li}}}{e_0} \sum_{i=1}^{N_{\mathtt{P}}} \tfrac{A^i_{\mathtt{E}}}{A_{\mathtt{E}}} \mu_{\mathrm{Li}}(y^i)\ . \end{aligned} \tag{123}$$

Finally we introduce the abbreviations

$$U^{\mathrm{ref}} = \tfrac{1}{e_0}\big(m_{\mathrm{Li^+}}\mu_{\mathrm{Li}^+_{\mathtt{A}}}|_{S_{\mathtt{A}}} + m_{\mathrm{e^-}}\mu_{\mathrm{e^-}}|_{S_{\mathtt{C}}} - m_{\mathrm{Li}}\mu^{\mathrm{ref}}_{\mathrm{Li}}\big) \tag{124}$$

and

$$\begin{aligned} & j^{\mathtt{P}}_{\mathrm{ic}} = \tfrac{e_0}{m_{\mathrm{Li}}} k_{\mathrm{Li}}\ , && j^{\mathtt{P}}_{\mathrm{ad}} = \tfrac{e_0 k_B T M^{\mathtt{E}}_{s,\mathrm{Li^+}}}{(m_{\mathrm{Li^+}})^2}\ , && j^{\mathtt{P}}_{\mathrm{re}} = e_0 k_B T R_0^{\mathtt{E}}\ , \\ & j^{\mathtt{A}}_{\mathrm{de}} = e_0 k_B T R_0^{\mathtt{AE}}\ , && j^{\mathtt{A}}_{\mathrm{ad}} = \tfrac{e_0 k_B T M^{\mathtt{AE}}_{s,\mathrm{Li^+}}}{(m_{\mathrm{Li^+}})^2}\ . \end{aligned} \tag{125}$$

Then we obtain a relation that relates the thermodynamic state of the electrochemical cell to the voltage,

$$U = U^{\mathrm{ref}} - \tfrac{m_{\mathrm{Li}}}{e_0} \sum_{i=1}^{N_{\mathtt{P}}} \tfrac{A^i_{\mathtt{E}}}{A_{\mathtt{E}}} \big(\mu_{\mathrm{Li}}(y^i) - \mu^{\mathrm{ref}}_{\mathrm{Li}}\big) - \tfrac{k_B T}{e_0} \tfrac{1}{A_{\mathtt{E}}} \Big(\tfrac{1}{j^{\mathtt{P}}_{\mathrm{ad}}} + \tfrac{1}{j^{\mathtt{P}}_{\mathrm{re}}} + \tfrac{1}{j^{\mathtt{P}}_{\mathrm{ic}}}\Big) I - \tfrac{k_B T}{e_0} \tfrac{1}{A_{\mathtt{AE}}} \Big(\tfrac{1}{j^{\mathtt{A}}_{\mathrm{de}}} + \tfrac{1}{j^{\mathtt{A}}_{\mathrm{ad}}}\Big) I\ . \tag{126}$$

7 Discussion and outlook

Noise is thermodynamically consistent introduced in the stochastic many-particle model. This is a remarkable feature because up to now there was no possibility to apply non-equilibrium thermodynamics [36, 7, 39] on a scale where stochastic fluctuations can be observed. For the first time we found that stochastic objects exclusively can be introduced within surface thermodynamics but not within non-equilibrium thermodynamics of the bulk. This fact fits to the observation that stochastic effects are more likely to influence surface phenomena rather than bulk phenomena. A prominent example concerns nucleation processes.

Due to our assumptions from Section 2, which are fulfilled by high power batteries, the relevant kinetic phenomena are reduced to pure surface phenomena. For this reason we are able to embody the complex charging-discharging process of a LFP electrode in a model of remarkable simplicity with few phenomenological parameters. The dynamics of the many-particle electrode is only controlled by two parameters: the intercalation rate k_{Li} and the strength of the stochastic fluctuations ν_0. Consequently the experimental determination of the two parameters is an easy task.

However, the battery voltage is controlled by further surface phenomena, viz. surface reaction, adsorption and deposition at the lithium anode. The careful derivation of the current-voltage relation (9) reveals that these three phenomena only lead to a shift of the voltage plateau in the voltage-current diagram if the charging rate changes. The magnitude of the shift is verified by measurements [41], see Figure 13. Thus the rate dependent capacity of the battery cannot originate from these surface phenomena. In our many-particle model, where diffusion is ignored within both particles and electrolyte, the rate dependent capacity can only originate from the intercalation of lithium into the iron phosphate lattice which is accompanied by phase transition within the many-particle ensemble of the electrode.

The many-particle model incorporates two different mechanisms for stochastic effects: (i) particle size distribution and (ii) stochastic fluctuations on the particle surfaces. From our simulations we conclude that the particle size distribution is the dominant stochastic effect in the electrode, particularly for the description of the battery voltage. An impact of the stochastic fluctuations on the phase transition is only observed in a slow charging regime. All simulations performed with a particle size distribution already show a pronounced phase separation. Moreover, the model is capable to predict the characteristic voltage plateaus of LFP electrodes. In the case of single size LFP particles stochastic fluctuations are necessary to initiate the phase transition but only in a very low charging regime. For moderate and fast charging regimes the single size particles behave identical and do not exhibit voltage plateaus.

A further prediction of our many-particle model concerns the ordering of the phase transition by the particle size: small particles undergo the phase transition first. However, the size distribution effect on the phase transition is less pronounced in experiments, [34], compared to the model. Certainly this

difference between experiments and model might be induced by our assumption of fast charge transport within the electrolyte. If the charge transport is limited by finite ion mobilities in the electrolyte, the phase transition would be more affected by the distance of the LFP electrode to the anode than by the size distribution of the LFP particles at least in thick electrodes.

Comparison with experimental data reveals that our many-particle model is capable to describe the voltage-capacity characteristic of real LFP batteries for different charging rates. Particularly the open-circuit potentials of the cell is predicted by the model.

Common battery models assume an electro-neutral electrolyte, which is not presumed in our many-particle model. Due to the assumption of fast charge transport within the electrolyte the electrochemical potentials are spatially constant. If the geometry of the electrode were known we could use the Poisson equation and the constant electrochemical potentials to determine both the electric potential and the charge distribution within the electrolyte. In particular, by means of suitable electrolyte models [16,17] the dimension of the electric double layer within the pore space of the LFP electrode could be studied. Then one could test if the assumption of electro-neutrality of the electrolyte in the pore space is appropriate.

The stochastic many-particle model of this study is derived in Section 6 from a more general and even more complex thermodynamic model for many-particle electrodes. About 23 assumptions on electrochemical processes where necessary to derive the simple stochastic many-particle model for the LFP electrode of Section 3. Already the comparison of simulation and experimental data suggest that processes like diffusion within the electrolyte cannot be ignored for high charging rates. However, the derivation in Section 6 gives us a systematic approach to extend the many-particle model in a consistent way to incorporate more phenomena like diffusion or heat transport.

The stochastic model of this paper is not restricted to a LFP electrode against a metallic lithium anode. For example, it is possible to replace the lithium anode with a graphite anode, Li_xC_6, or lithium titanium oxide anode, $Li_4Ti_5O_{12}$ that is likewise to be represented by a many-particle model. In this setting simulations of commercial cells with the many-particle model become possible.

Acknowledgements This research was supported by the Research Center MATHEON through project C-SE8 funded by the Einstein Center for Mathematics Berlin.

List of symbols many particle model

U	[V]	- reference potential
k_{Li}	[kg/m^{2}s]	- lithium intercalation rate
j_{P}	[A/m^2]	- exchange current
ν_0	[m$^{\frac{3}{2}}$]	- stochastic strength
L	[J]	- heat of solution
A^i	[m^2]	- particle surface area
A^i_{E}	[m^2]	- active surface area
V^i	[m^3]	- particle volume
V_{P}	[m^3]	- total volume
A_{E}	[m^2]	- total active area
y^i, Y^i		- lithium mole fraction
τ^i	[s]	- relaxation time
ν^i		- stochastic strength

List of symbols

k_B	[J/K]	- Boltzmann constant
e_0	[C]	- elementary charge
ε_0	[C/(V m)]	- electric constant
z_α		- charge number
m_α	[kg]	- molecular mass
γ^i_α, $\gamma^i_{s,\alpha}$		- stoichiometric coef. bulk and surface reactions
$\boldsymbol{\nu}$		- normal vector
k_M	[1/m]	- mean curvature
T,T_s	[K]	- bulk and surface temperature
n_α	[m^{-3}]	- bulk number density
$n_{s,\alpha}$	[m^{-2}]	- surface number density
ρ_α	[kg/m^3]	- bulk mass density
$\rho_{s,\alpha}$	[kg/m^2]	- surface number density
$\boldsymbol{v}$, $\boldsymbol{v}_s$	[m/s]	- bulk and surface barycentric velocity
$\boldsymbol{w}$	[m/s]	- surface velocity
$\boldsymbol{E}$	[V/m]	- electric field
φ, φ_s	[V]	- bulk and surface electrostatic potential
n^{F}	[C/m^3]	- charge density
n^{F}_s	[C/m^2]	- surface charge density
$\rho\psi$	[J/m^3]	- free energy density
$\rho_s\psi_s$	[J/m^2]	- surface free energy density
μ_α, $\mu_{s,\alpha}$	[J/kg]	- bulk and surface chemical potential
$\boldsymbol{\sigma}$	[N/m^2]	- Cauchy stress tensor
$\boldsymbol{\Sigma}$	[N/m^2]	- total stress tensor
p	[N/m^2]	- material pressure
γ_s	[N/m]	- surface tension
$\boldsymbol{J}_\alpha$	[kg/sm^2]	- mass flux density
$\boldsymbol{J}_{s,\alpha}$	[kg/sm^2]	- surface mass flux density
$\boldsymbol{j}_\alpha$	[kg/sm^2]	- total mass flux density
$\boldsymbol{J}_{s,\alpha}$	[kg/sm]	- surface mass flux density
$\boldsymbol{j}_{s,\alpha}$	[kg/sm]	- total surface mass flux density
R^i	[1/sm^3]	- bulk reaction rate density
R^i_s	[1/sm^2]	- surface reaction rate density
r^i	[kg/sm^3]	- bulk mass production density
r^i_s	[kg/sm^2]	- surface mass production density

References

1. Bai, P., Cogswell, D., Bazant, M.: Suppression of phase separation in $LiFePO_4$ nanoparticles during battery discharge. Nano Lett. **11**(11), 4890–4896 (2011)
2. Bazant, M.Z.: Theory of chemical kinetics and charge transfer based on nonequilibrium thermodynamics. Accounts Chem. Res. **46**(5), 1144–1160 (2013)
3. Bedeaux, D.: Nonequilibrium thermodynamics and statistical physics of surfaces. In: P. Ilya, S.A. Rice (eds.) Advances in Chemical Physics, vol. 64, pp. 47–109. John Wiley Sons, Inc. (1986)
4. Bothe, D., Dreyer, W.: Continuum thermodynamics of chemically reacting fluid mixtures. Acta Mech. pp. 1–49 (2014)
5. Chueh, W., El Gabaly, F., Sugar, J., Bartelt, N., McDaniel, A., Fenton, K., Zavadil, K., Tyliszczak, T., Lai, W., McCarty, K.: Intercalation pathway in many-particle LiFePO4 electrode revealed by nanoscale state-of-charge mapping. Nano Letters **13**(3), 866–872 (2013)
6. Costen, R., Adamson, D.: Three-dimensional derivation of the electrodynamic jump conditions and momentum-energy laws at a moving boundary. Proceedings of the IEEE **53**(9), 1181–1196 (1965)
7. deGroot, S.R., Mazur, P.: Non-Equilibrium Thermodynamics. North Holland, Amsterdam (1963)
8. Delmas, C., Maccario, M., Croguennec, L., Le Cras, F., Weill, F.: Lithium deintercalation in $LiFePO_4$ nanoparticles via a domino-cascade model. Nature Materials **7**, 665–671 (2008)
9. Dominko, R., Bele, M., Gaberšček, M., Remskar, M., Hanzel, D., Pejovnik, S., Jamnik, J.: Impact of the carbon coating thickness on the electrochemical performance of LiFePO4/C composites. Journal of The Electrochemical Society **152**(3), A607–A610 (2005)
10. Doyle, M., Fuller, T., Newman, J.: Modeling of galvanostatic charge and discharge of the lithium/polymer/insertion cell. Journal of The Electrochemical Society **140**(6), 1526–1533 (1993)
11. Doyle, M., Newman, J.: Analysis of capacity-rate data for lithium batteries using simplified models of the discharge process. Journal of Applied Electrochemistry **27**(7), 846–856 (1997)
12. Dreyer, W., Friz, P., Gajewski, P., Guhlke, C., Maurelli, M.: to be published. WIAS Preprint (2017)
13. Dreyer, W., Gaberšček, M., Guhlke, C., Huth, R., Jamnik, J.: Phase transition in a rechargeable lithium battery. European Journal of Applied Mathematics **22**, 267–290 (2010)
14. Dreyer, W., Guhlke, C., Herrmann, M.: Hysteresis and phase transition in many-particle storage systems. Continuum Mech. Thermodyn. **23**(3), 211–231 (2011)
15. Dreyer, W., Guhlke, C., Huth, R.: The behavior of a many-particle electrode in a lithium-ion battery. Physica D: Nonlinear Phenomena **240**(12), 1008–1019 (2011)
16. Dreyer, W., Guhlke, C., Müller, R.: Overcoming the shortcomings of the Nernst–Planck model. Phys. Chem. Chem. Phys. **15**, 7075–7086 (2013)
17. Dreyer, W., Guhlke, C., Müller, R.: Modeling of electrochemical double layers in thermodynamic non-equilibrium. Phys. Chem. Chem. Phys. **17**, 27,176–27,194 (2015)
18. Dreyer, W., Guhlke, C., Müller, R.: A new perspective on the electron transfer: recovering the Butler-Volmer equation in non-equilibrium thermodynamics. Phys. Chem. Chem. Phys. **18**, 24,966–24,983 (2016)
19. Dreyer, W., Huth, R., Mielke, A., Rehberg, J., Winkler, M.: Global existence for a nonlocal and nonlinear Fokker–Planck equation. Zeitschrift für angewandte Mathematik und Physik **66**(2), 293–315 (2015)
20. Dreyer, W., Jamnik, J., Guhlke, C., Huth, R., Moškon, J., Gaberšček, M.: The thermodynamic origin of hysteresis in insertion batteries. Nature Materials **9**, 448–453 (2010)
21. Farkhondeh, M., Delacourt, C.: Mathematical modeling of commercial LiFePO4 electrodes based on variable solid-state diffusivity. Journal of The Electrochemical Society **159**(2), A177–A192 (2011)

22. Farkhondeh, M., Pritzker, M., Fowler, M., Safari, M., Delacourt, C.: Mesoscopic modeling of li insertion in phase-separating electrode materials: application to lithium iron phosphate. Phys. Chem. Chem. Phys. **16**, 22,555–22,565 (2014)
23. Farkhondeh, M., Safari, M., Pritzker, M., Fowler, M., Han, T., Wang, J., Delacourt, C.: Full-range simulation of a commercial LiFePO4 electrode accounting for bulk and surface effects: A comparative analysis. Journal of The Electrochemical Society **161**(3), A201–A212 (2014)
24. Fournier, N., Hauray, M., Mischler, S.: Propagation of chaos for the 2D viscous vortex model. J. Eur. Math. Soc. (JEMS) **16**(7), 1423–1466 (2014)
25. Franco, A.: Multiscale modelling and numerical simulation of rechargeable lithium ion batteries: concepts, methods and challenges. RSC Advances **3**, 13,027–13,058 (2013)
26. Guhlke, C.: Theorie der elektrochemischen Grenzfläche. Ph.D. thesis, TU-Berlin (2015)
27. Han, B., Van der Ven, A., Morgan, D., Ceder, G.: Electrochemical modeling of intercalation processe with phase field models. Electrochim. Acta **49**, 4691–4699 (2004)
28. Hellwig, C., Sörgel, S., Bessler, W.: A multi-scale electrochemical and thermal model of a LiFePO4 battery. ECS Transactions **35**(32), 215–228 (2011)
29. Herrmann, M., Niethammer, B., Velázquez, J.: Kramers and non-kramers phase transitions in many-particle systems with dynamical constraint. SIAM Multiscale Model. Simul. **10**(3), 818–852 (2012)
30. Herrmann, M., Niethammer, B., Velázquez, J.: Rate-independent dynamics and Kramers-type phase transitions in nonlocal Fokker-Planck equations with dynamical control. Arch. Ration. Mech. Anal. **124**(3), 803–866 (2014)
31. Latz, A., Zausch, J.: Thermodynamic consistent transport theory of Li-ion batteries. J. Power Sources **196**(6), 3296–3302 (2011)
32. Latz, A., Zausch, J.: Thermodynamic derivation of a Butler Volmer model for intercalation in Li-ion batteries. Electrochim. Acta (2013)
33. Li, Y., El Gabaly, F., Ferguson, T., Smith, R., Bartelt, N., Sugar, J., Fenton, K., Cogswell, D., Kilcoyne, A., Tyliszczak, T., Bazant, M., Chueh, W.: Current-induced transition from particle-by-particle to concurrent intercalation in phase-separating battery electrodes. Nature Materials **13**, 1476–1122 (2014)
34. Li, Y., Meyer, S., Lim, J., Lee, S., Gent, W., Marchesini, S., Krishnan, H., Tyliszczak, T., Shapiro, D., Kilcoyne, A., Chueh, W.: Effects of particle size, electronic connectivity, and incoherent nanoscale domains on the sequence of lithiation in LiFePO4 porous electrodes. Advanced Materials **27**(42), 6591–6597 (2015)
35. Li, Y., Weker, J., Gent, W., Mueller, D., Lim, J., Cogswell, D., Tyliszczak, T., Chueh, W.: Dichotomy in the lithiation pathway of ellipsoidal and platelet LiFePO4 particles revealed through nanoscale operando state-of-charge imaging. Advanced Functional Materials **25**(24), 3677–3687 (2015)
36. Meixner, J., Reik, H.G.: Thermodynamik der irreversiblen Prozesse, vol. 3, pp. 413–523. Springer, Berlin (1959)
37. Mielke, A., Truskinovsky, L.: From discrete visco-elasticity to continuum rate-independent plasticity: Rigorous results. Archive for Rational Mechanics and Analysis **203**(2), 577–619 (2012)
38. Moskon, J., Dominko, R., Cerc-Korosec, R., Gaberšček, M., Jamnik, J.: Morphology and electrical properties of conductive carbon coatings for cathode materials. J. Power Sources **174**(2), 683–688 (2007)
39. Müller, I.: Thermodynamics, Interaction of Mechanics and Mathematics Series. Pitman Advanced Publishing Program, Boston (1985)
40. Padhi, A., Nanjundaswamy, K., Goodenough, J.: Phospho-olivines as positive-electrode materials for rechargeable lithium batteries. J. Electrochem. Soc. **144**, 1188–1194 (1997)
41. Safari, M., Delacourt, C.: Mathematical modeling of lithium iron phosphate electrode: Galvanostatic charge/discharge and path dependence. Journal of The Electrochemical Society **158**(2), A63–A73 (2011)
42. Singh, G., Ceder, G., Bazant, M.: Intercalation dynamics in rechargeable battery materials: General theory and phase-transformation waves in LiFePO4. Electrochimica Acta **53**(26), 7599 – 7613 (2008)
43. Srinivasan, V., Newman, J.: Discharge model for the lithium iron-phosphate electrode. Journal of The Electrochemical Society **151**(10), A1517–A1529 (2004)

44. Sznitman, A.S.: Topics in propagation of chaos. In: École d'Été de Probabilités de Saint-Flour XIX—1989, *Lecture Notes in Math.*, vol. 1464, pp. 165–251. Springer, Berlin (1991)